



Lawrence Berkeley Laboratory

UNIVERSITY OF CALIFORNIA

Materials & Molecular Research Division

SLIDING MECHANISMS FOR GRAIN BOUNDARIES CONTAINING
PRE-EXISTING CAVITIES IN Al_2O_3 - SiO_2 CERAMICS

Amar Pal Singh Rana
(Ph.D. thesis)

November 1980

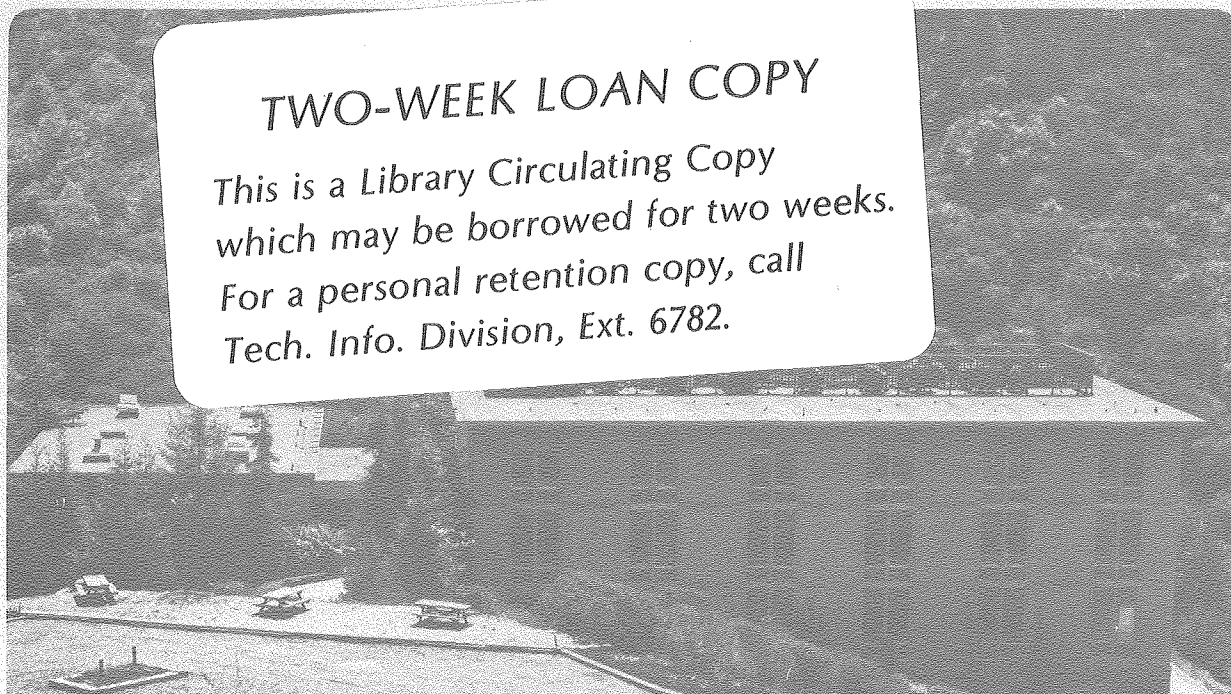
RECEIVED
LAWRENCE
BERKELEY LABORATORY

JAN 2 1981

LIBRARY AND
DOCUMENTS SECTION

TWO-WEEK LOAN COPY

This is a Library Circulating Copy
which may be borrowed for two weeks.
For a personal retention copy, call
Tech. Info. Division, Ext. 6782.



LBL-11486 e.2

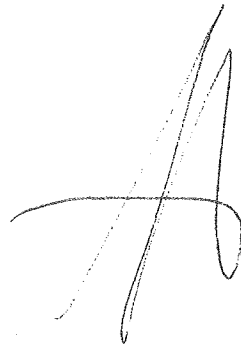
DISCLAIMER

This document was prepared as an account of work sponsored by the United States Government. While this document is believed to contain correct information, neither the United States Government nor any agency thereof, nor the Regents of the University of California, nor any of their employees, makes any warranty, express or implied, or assumes any legal responsibility for the accuracy, completeness, or usefulness of any information, apparatus, product, or process disclosed, or represents that its use would not infringe privately owned rights. Reference herein to any specific commercial product, process, or service by its trade name, trademark, manufacturer, or otherwise, does not necessarily constitute or imply its endorsement, recommendation, or favoring by the United States Government or any agency thereof, or the Regents of the University of California. The views and opinions of authors expressed herein do not necessarily state or reflect those of the United States Government or any agency thereof or the Regents of the University of California.

SLIDING MECHANISMS FOR GRAIN BOUNDARIES CONTAINING
PRE-EXISTING CAVITIES IN $\text{Al}_2\text{O}_3\text{-SiO}_2$ CERAMICS

Amar Pal Singh Rana
(*Ph.D. thesis*)

November 1980

A handwritten signature in black ink, consisting of a large, stylized capital 'A' with a horizontal crossbar and a vertical stroke that loops around to the left.

SLIDING MECHANISMS FOR GRAIN BOUNDARIES CONTAINING
PRE-EXISTING CAVITIES IN Al_2O_3 - SiO_2 CERAMICS

Amar Pal Singh Rana

Materials and Molecular Research Division
Lawrence Berkeley Laboratory
and
Department of Materials Science and Mineral Engineering
University of California
Berkeley, California 94720

This work was supported by the U.S. Department of Energy
Under Contract No. W-7405-ENG-48

TABLE OF CONTENTS

Abstract	v
Acknowledgments.	vii
1. Introduction	1
2. Total Sliding From Elastic Accommodation	3
2.1. Stress Intensity Factor Solutions	3
2.2. Additional Elastic Accommodation	5
3. Transient Sliding.	6
4. Grain Boundary Viscosity	8
4.1. Single Phase Microstructure.	8
4.2. Continuous Second Phase.	8
5. The Relaxation Time.	15
6. Experimental Method.	16
6.1. Materials.	16
6.2. Vacuum Hot Pressing.	19
6.3. Properties	20
6.4. Modulus of Elasticity Measurements	22
6.5. Internal Friction Measurements	24
a. Identification of the vibrating mode	28
b. Suspension system.	31
c. Transducers.	32
d. High temperature measurements.	33
7. Results and Discussion	47
7.1. The Damping Spectra.	47
7.2. Comparison of Results With Theory.	47

TABLE OF CONTENTS (cont)

8. High Temperature Background.	52
8.1. Introduction	52
8.2. Grain Boundary Sliding	53
9. Summary and Conclusions.	61
Appendix A: Relaxed Stress Distribution	62
References	63
Figure Captions.	72
Figures	75

SLIDING MECHANISMS FOR GRAIN BOUNDARIES CONTAINING
PRE-EXISTING CAVITIES IN $\text{Al}_2\text{O}_3\text{-SiO}_2$ CERAMICS

Amar Pal Singh Rana

Materials and Molecular Research Division
Lawrence Berkeley Laboratory
and
Department of Materials Science and Mineral Engineering
University of California
Berkeley, California 94720

ABSTRACT

High temperature failure in ceramics frequently involves the nucleation, growth and coalescence of grain boundary located microcracks or cavities. Fabrication processes such as hot pressing and sintering also lead to the presence of cavities at grain boundaries. The intent of this study is to examine models of grain boundary sliding when cavities are present at grain boundaries in $\text{Al}_2\text{O}_3\text{-SiO}_2$ ceramics using the internal friction technique.

Internal friction is the dissipation of energy that occurs when stress and strain are not in phase. An apparatus was developed to measure internal friction and elastic modulus up to 1200°C using a sonic resonance technique, with electromagnetic transducers. In a polycrystal, small amounts of total sliding (strains $\sim 10^{-4}$) can be accommodated by elastic strains in the neighboring grains. The sliding is recoverable and is accumulated and discharged with a characteristic relaxation time which is a function of grain boundary viscosity. This relaxation time can be measured in an internal friction experiment.

Models of high temperature deformation in ceramics must recognize the various microstructures that typically occur, particularly the presence of second phases at grain boundaries. Two types of microstructure, and the concomitant modes of grain boundary sliding, were distinguished in this study. The first microstructure consisted of grains encompassed by an amorphous phase. The relaxation time has been calculated when grain boundaries have pre-existing cavities. Sliding in single phase microstructure is accommodated by boundary diffusion and by viscous deformation in materials with a glassy grain boundary phase. Relaxation times derived from internal friction measurements were shown to be in fair agreement with theoretical relaxation times. Cavities only had a small contribution to grain boundary sliding.

At relatively high temperatures, internal friction rises exponentially to very large values. This phenomenon (referred to as the high temperature background) is manifest in polycrystalline samples as an upturn in the internal friction on the high temperature side of the peak. A transient analysis pertinent to the high temperature background demonstrated the significance of a dimensionless parameter, which was a function of frequency, grain size, elastic modulus and grain boundary diffusivity.

ACKNOWLEDGMENTS

I wish to express my sincere appreciation to Professor Anthony G. Evans for his continuous guidance and support in this research work. I also wish to express my deepest gratitude to Professor Joseph A. Pask, under whose able guidance this work got started. Thanks are due to Professor Ian Finnie for reviewing this manuscript and providing necessary help to develop this research.

Acknowledgments are extended to my colleagues and friends and to Shirley Ashley and her staff at TID for typing.

This work was supported by the U.S. Department of Energy under Contract No. W-7405-ENG-48.

CHAPTER 1

INTRODUCTION

Many polycrystals of refractory materials such as alumina, mullite, metallic carbides, etc. are made by sintering at high temperatures. The last vestiges of porosity must often be eliminated if the highest strengths are to be obtained, but this is hard to achieve. There are sufficient observations^{1,2} to indicate that high temperature fracture in ceramics frequently involves the nucleation, growth and coalescence of grain boundary located microcracks or cavities. The propagation of individual cavities or cavity arrays, either by diffusion³⁻⁷ or by viscous flow⁸ of a boundary phase, is well understood. Coupled cavity propagations and coalescence effects that dictate the final failure have also been examined.⁹ The intent of the present paper is to examine models of grain boundary sliding when pre-existing cavities are present at grain boundaries in $\text{Al}_2\text{O}_3\text{-SiO}_2$ ceramics using internal friction techniques.

In a polycrystal, grain boundary sliding can be accommodated by elastic deformation of the grains. Presence of pre-existing cavities at grain boundaries cause additional sliding. This sliding is recoverable upon removal of applied stress and is accumulated and discharged with a characteristic relaxation time which is a function of the viscosity of the grain boundary in the presence of pre-existing cavities. This relaxation time can be measured in an internal friction experiment.

Models of high temperature deformation in ceramics must recognize the various microstructures that typically occur, particularly the presence and dispersion of second phases at grain boundaries. Two types

of microstructure, and the concomitant modes of grain boundary sliding will be distinguished in the present paper. The first microstructure is one with no second phase at grain boundaries (i.e., a single phase material). Mullite (75 wt.% Al_2O_3) was chosen for this purpose. For this case sliding is accommodated by grain boundary diffusion and the material displaced from pre-existing cavities being accommodated at grain boundaries and vice-versa, causing mode I displacements.

The second microstructure consists of grains encompassed by an amorphous second phase with pre-existing cavities, typical of many ceramics fabricated by hot pressing or sintering. For this case, sliding is accommodated by viscous flow and the material displaced from pre-existing cavities being accommodated at grain boundaries and vice versa causing mode I displacements.

The relaxation time was calculated using a procedure described here in for the two microstructures described. Internal friction experiments were performed to measure these relaxation times. Satisfactory agreement was obtained with the analytic results. The measurements also confirmed the theoretically predicted dependence of boundary viscosity upon pre-existing cavity size and spacing and the grain size.

CHAPTER 2

TOTAL SLIDING FROM ELASTIC ACCOMMODATION

Consider a polycrystal containing pre-existing cavities at the grain boundaries. When a stress lower than the yield stress is applied to the polycrystal the following happens: First, there is an instantaneous elastic deformation. Second, pre-existing cavities at grain boundaries cause additional sliding. As elastic boundaries begin to slide, further elastic deformation of the grains occur, back stresses opposing the sliding build up and the sliding comes to a halt. This is sliding by elastic accommodation.

2.1. Stress Intensity Factor Solutions

The extension of a wedge crack that emanates at a triple point has previously been analysed using a cracked dislocation solution first proposed by Stroh¹⁰ and extended by Cottrell.¹¹ This solution can be demonstrated to exhibit the form

$$\kappa \tau_s \sqrt{l} = \tau_s \sin 2\phi \sqrt{\pi(a/2)} + \frac{hE}{\sqrt{2\pi a(1-\nu^2)}} \quad (2.1)$$

where $2h$ is the wedge opening, a is the crack length, $\kappa(=K/\tau_s \sqrt{l})$ is the normalized stress intensity factor, E is Young's modulus, $2l$ is facet length and τ_s is the shear stress at grain boundary. The first term is due to the normal opening of the crack K_O and the second derives from the wedge opening produced by sliding K_w . However, this solution is inadequate for the complete description of the wedge crack extension; because the wedge opening h cannot be specified a priori (steady state sliding will not occur in the present problem). A comparison solution

that provides the requisite complementary information can be derived from recent stress intensity solutions for the kinked crack,¹² with the kink at an inclination $\phi(=2\theta)$ to the sliding boundary Fig. 2-1). The pertinent stress intensity factors are deduced by regarding the primary crack as being subjected to a pure shear stress τ (Fig. 2-1) plus a small superimposed crack surface traction to prevent opening of the primary crack.

The mode I and II stress intensity factors provided by the analysis are then combined in accord with the coplanar strain energy release rate criterion to obtain the driving force K for coplanar wedge crack extension, as;

$$K = \left(K_I^2 + K_{II}^2 \right)^{1/2} \quad (2.2)$$

The results, plotted in terms of the normalized stress intensity factor $\kappa(=K/\tau\sqrt{\ell})$ are shown in Figure 2-1. Rearranging Eq. (2.1), we have

$$h = \frac{\sqrt{2\pi a} (1-\nu^2)}{E} \left(\kappa \tau_s \sqrt{\ell} - \tau_s \sin 2\phi \sqrt{\pi(a/2)} \right) \quad (2.3)$$

The average sliding displacement $\langle u \rangle$ due to cavities at triple points is related to wedge opening h by

$$\langle u \rangle = \frac{\pi}{4} h \operatorname{cosec} \phi \quad (2.4)$$

Thus

$$\langle u \rangle_{\substack{\text{triple} \\ \text{point} \\ \text{cavities}}} = \frac{\pi}{4E} \operatorname{cosec} \phi \sqrt{2\pi a} (1-\nu^2) \tau_s \left[\kappa \sqrt{\ell} - \sin 2\phi \sqrt{\pi(a/2)} \right] \quad (2.5)$$

2.2. Additional Elastic Accommodation

Further we note that the elastic displacement $\langle u \rangle$ of a mode II crack (length 2ℓ) subjected to uniform shear values with distance x from the center as¹³

$$u(x) = \frac{4\tau_s(1-\nu^2)(\ell^2-x^2)^{1/2}}{\pi E} \quad (2.6)$$

The average displacement is thus;

$$\langle u \rangle = \tau_s \ell (1-\nu^2)/E \quad (2.7)$$

For comparison, we have from Eqs. (2.5) and (2.7)

$$\frac{\langle u \rangle_{\text{tpc}}}{\langle u \rangle} = \left(\frac{\pi}{2} \right)^{3/2} \text{cosec } \phi \left(\frac{a}{\ell} \right)^{1/2} \left[\kappa - \sin 2\phi \left(\frac{\pi}{2} \cdot \frac{a}{\ell} \right)^{1/2} \right] \quad (2.8)$$

Which is plotted in Fig. 2-2. It is thus seen that for small values of a/ℓ , typical of experiments, the contribution from triple point cavities is small.

CHAPTER 3

TRANSIENT SLIDING

The total sliding \bar{U} as a result of an applied stress τ_a is given by adding displacements from Eqs. (2.5) and (2.7). Thus we have

$$\bar{U} = \frac{\tau_a \cos\phi (1-\nu^2)}{E} \left[1 + \frac{F}{\ell} \cdot \frac{\pi}{4} \operatorname{cosec}\phi \sqrt{2\pi a} \left(\kappa\sqrt{\ell} - \sin 2\phi \sqrt{\pi(a/2)} \right) \right] \quad (3.1)$$

where F is a fraction of triple points containing pre-existing cavities. The normal stress σ_n at the sinusoidal boundary of wavelength λ ($=3d/2$) as a result of applied stress τ_a is given by

$$\sigma_n = - \frac{6\tau_a}{\pi} \sin \frac{2\pi}{\lambda} y \quad (3.2)$$

The shear stress across the boundary at time t is given by

$$\tau_s(t) = \tau_a - \frac{2}{\lambda} \int_0^\lambda \sigma_n(t) \tan\theta \cdot dy \quad (3.3)$$

where $\tan\theta$ is the slope of the sinusoidal boundary represented by:

$$x = \frac{d}{2} \cos \frac{2\pi}{\lambda} y \quad (3.4)$$

From Eqs. (3.1) and (3.3) we obtain

$$\tau_s(t) = \tau_a - \beta U(t) \quad (3.5)$$

where

$$\beta = \frac{2E}{(1-\nu^2) \cos\phi \cdot \ell} \left[1 + \frac{F}{\ell} \cdot \frac{\pi}{4} \operatorname{cosec}\phi \sqrt{2\pi a} \left(\kappa\sqrt{\ell} - \sin 2\phi \sqrt{\pi(a/2)} \right) \right]^{-1} \quad (3.6)$$

expression for β for fully dense material can be obtained by deleting last two terms in the denominator. Using the equation for boundary viscosity η and taking δ as the boundary thickness

$$\frac{\dot{U}(t)}{\delta} = \frac{\tau_s(t)}{\eta} \quad (3.7)$$

and combining with Eq. (3.5) leads to

$$\dot{U} = (\tau_a/\beta - U)\delta\beta/\eta \quad (3.8)$$

The solution to which is

$$U(t) = \frac{\tau_a}{\beta} (1 - e^{-t/\tau}) \quad (3.9)$$

where the relaxation time

$$\tau = \eta/\delta\beta \quad (3.10)$$

CHAPTER 4

GRAIN BOUNDARY VISCOSITY

In a fully dense material, the characteristic relaxation time is a function of intrinsic viscosity of grain-boundary. When pre-existing cavities are present at grain boundaries, the material displaced from the cavities can be accommodated at grain boundaries and vice-versa causing mode I displacements. The contribution of pre-existing cavities is calculated for the two microstructures.

4.1. Single Phase Microstructure

In this case the growth of pre-existing cavities involves grain boundary diffusion with the material displaced from the cavities being accommodated at grain boundaries. Such an accommodation mechanism permits only small mode I displacements and small cavity surface separations.

4.2. Continuous Second Phase

Two essentially different mechanisms have been proposed to describe the growth of grain boundary voids. The diffusive growth models of Hull and Rimmer¹ and Balluffi and Seigle² consider the cavity to be fed by a flux of vacancies generated in the grain boundary by the applied stress; the other view has not been quantified but assumes that the cavity behaves as a shear crack which grows by grain boundary sliding (Gifkins³ and Chen and Machlin.⁴ Both viewpoints owe their viability to certain key experiments which appear to support one mechanism and exclude the other. Important observations supporting a deformation growth process are, e.g., the ability of alloying elements to reduce both creep rate and rupture life whilst having little effect on diffusion (5.6) and the ability of cavities to grow under a compressive applied stress.^{1,8}

The outstanding evidence for the diffusion mechanism is the inhibition of cavity growth on application of hydrostatic pressure equal to applied stress⁹. Evans¹⁰ approach was to add the total energy of the system in a manner similar to that used by Cottrell¹¹ and Gilman¹² for cracked dislocation and adapted by Williams¹³ for high temperature wedge cracking the cavity was treated as a hollow dislocation. Evans¹⁰ assumed that matrix was sufficiently plastic to accommodate the misfit strains produced during the growth of the cavity. Evans¹⁰ showed that the cavity growth can occur only by grain boundary sliding and that sliding cannot occur without concurrent cavity growth.

Further there is an incomplete amount of evidence (in the opinion of Gifkins¹⁴ in a 1963 review) in favor of the vacancy condensation model, where grain boundary diffusion is the principal path. A number of objections have raised to the model to favor strain-controlled growth. Apart from the early comments of Nield and Quarrel¹⁵ and Chen and Machlin,¹⁶ Kramer and Machlin¹⁷ found that creep strain and void area are linearly related in nickel. This rules out vacancy controlled void growth. Although the creep process itself is reported^{18,19} to be dominated in this metal by a vacancy-producing mechanism.

Another objection to vacancy growth originates in the study of Intrater and Machlin.²⁰ Working in a temperature range of 650° to 900°C, they found that the area of visible voids was independent of temperature. In dilute alloys a linear relation between void volume and strain has been reported by Bowring et al.⁶, although Magnox AL 80 the linearity was only achieved late in the creep life. Linearity with creep strain

was also noted by Hensler and Cullen²¹ in a series of magnesium alloys. They found the effect to decrease with decreasing grain size.

The effect of pre-existing voids was studied by Davies and Denison²² who compared samples produced by powder-metallurgical techniques (purposely to contain voids) with fully dense vacuum cast samples of the same material. They showed the time to failure vs strain rate relationship to hold independently of stress and temperature. They went on to assume that creep life had been reduced through an increased creep rate. This results from the presence of voids which drain off any excess vacancies. The results also support those of Kramer and Machlin¹⁷ on the void fraction vs creep strain relationship and reflect the independence of creep rate from vacancy controlled growth.

Gittins²³ pointed out that cavitation rate at high strain rates was probably controlled by grain boundary sliding²⁴ and at low strain rates by a combination of sliding and vacancy accumulation.²⁵ In response to these comments, Davies and Williams²⁶ had shown that vacancy loss can be superceded by deformation controlled growth. They do not accept that a vacancy contribution is significant in cavity growth.

In view of the increasing amount of discussion in terms of a dominant controlling process, attempts have been made to find a transition from vacancy to deformation controlled growth. Day²⁷ was unable to distinguish between them in steel, nor were Chen and Machlin¹⁶ in their early work with brass. The strain rate-dependent void growth (with respect to tensile axis) found by Gittins and Williams²⁸ was cited as evidence for such a transition but was criticized, and referred to a change in mode of deformation controlled by Taplin.²⁹

A change in control of growth has also been sought by Evans.³⁰ Working with a dilute magnesium-aluminum alloy, he concluded that growth was dominated by grain-boundary sliding. The rate of increase of void length is directly related to the sliding. The minimum in ductility is attributed to a maximum void growth rate and its parallel maximum sliding rate. The sliding rate at higher temperatures is decreased by the formation of grain-boundary cusps. A minimum in the relation between creep rate and grain size was reported by Wilshire.³¹ He found that it increased as the temperature increased and again discussed the effect in terms of the increasing importance of grain boundary sliding with increasing grain size.

The review of Greenwood³² tends to support vacancy accretion in the light of experiments involving hydrostatic pressure. However, these experiments are not without critics. Machlin³³ has given an alternative explanation. Taplin³⁴ gives support to the possible role of vacancies at low strain rates. In contrast Wilshire,³⁵ writing in 1973, tended to negate the evidence for vacancy growth because of the results of reversed stressing experiments. If it is accepted that several mechanisms are possible, then evidence that vacancy absorption by voids and their resultant growth is nevertheless persuasive. Evidence in favor of deformation controlled growth is far stronger. The non-sphericity of cavities, the need for tension across the boundaries to avoid sintering, the temperature independence of void growth, the marked effect of alloying which does not alter the diffusion coefficient, all can be cited^{14,32,34,35} in support. In addition, the relation between cavitation and creep strain, and between the rate of change of both and creep life is also

indicative of deformation controlled growth.³⁵ Finally there is a good case to be made for several types of deformation-controlled growth.³⁴

According to Hancock,³⁶ in a creeping solid holes may grow by vacancy condensation or by the action of the applied stress producing strains at the surface of the hole which cause it to grow. The latter mechanism does not involve a vacancy flux to the hole. A comparison of the two processes indicated the conditions under which hole growth without vacancy condensation is faster than hole growth by diffusion. Low values of the ratio $\sigma/\dot{\epsilon}$, where σ is stress and $\dot{\epsilon}$ is the strain rate as well as large voids favor the strain process.

Several authors have examined the problem of brittle cracking along grain boundaries during creep.⁴¹⁻⁴⁴ These studies have generally commenced from the premise that grain boundary sliding will be occurring at a specified rate, $\dot{u}_{g.b.s.}$, and that the resultant sliding displacements provide the impetus for extension of a brittle wedge crack.

However, a prescribed steady state grain boundary sliding can only be occurring if the sliding is everywhere accommodated either by diffusion⁴⁵ or, perhaps by cracking. If it is implicitly assumed that diffusional accommodation is occurring, then it must be appreciated that diffusion will also modify the configuration of the crack tip.³⁷⁻³⁹ In fact, the crack (which becomes a cavity) will extend by diffusion, in accordance with the descriptions outlined by Chuang, et al.;^{37,40} Vitek³⁸ and Speight et al.³⁹ The earlier models⁴¹⁻⁴³ used linear elastic wedge opening solutions to describe the crack length and are thus not pertinent to conditions which involve diffusion. The presence of a steady state boundary sliding displacement to extend the crack is thus ambivalent.

It was subsequently recognized⁴⁴ that a wedge crack, once initiated, is likely to extend by diffusion, whenever diffusive conditions exist; and an approximate analysis of diffusive extension was presented.

An interesting attempt to produce a model in which both deformation within the grains and vacancy accretion play a role has been made by Ishida and McLean.⁴⁸ They envisage dislocations moving down slip lines within the grains to intersect a grain boundary. Under the action of the tensile stress, they migrate along the boundary which can only be done by climb (still retaining their burgers vectors). The vacancies emitted during climb process migrate to a growing cavity. The dislocation also exerts a force on this cavity, tending to open it, which is proportional to the distance between cavities. This model is of particular interest because it relates growth to grain boundary sliding. This model has been invoked to explain experimental observations in dilute nickel and magnesium alloys by Bowrig et al.⁶ and in copper and steel by Johannesson and Thölen.²⁴

A more detailed analysis based on recent 'crack line' cavity extension concepts³⁷⁻³⁹ is needed to afford a thorough description of the failure process. In the present analysis diffusion is not admitted and the only permissible viscous motion is grain boundary sliding. Brittle cracks are then tenable. The occurrence of this condition must be limited (since grain boundary sliding itself usually involves diffusive processes, because of the presence of ledges and of non-planarity), but important situations can be conceived wherein the proposed process might be encountered. For example, ceramics prepared by liquid phase sintering often have planar boundaries, and contain a second phase at the

boundaries. Thus the growth of pre-existing cavities involves mass transport by viscous flow with the material displaced from the cavity being accommodated at grain boundary.

CHAPTER 5

THE RELAXATION TIME

The relaxation time which is a function of the viscosity of grain boundary can now be calculated separately for the two microstructures. This relaxation time can be measured in an internal friction experiment.

5.1. Equi-axed Single Phase Microstructure

In this case the relaxation time can be calculated from Eqs. (3.6) and (3.10). Thus we have

$$\frac{\tau \cos\theta}{d \cos 2\theta} = (\eta/\delta) \frac{3(1-\nu^2)}{16E} \frac{1 + 2F \cos\theta \cdot \pi \operatorname{cosec} 2\theta}{d} (\kappa(3d/8\cos\theta))^{1/2} - \sin 4\theta (\pi a/2)^{1/2} \quad (5.1)$$

5.2. Continuous Second Phase

In this case the relaxation time can be calculated from Eqs. (3.6) and (3.10) and we get Eq. (5.1).

CHAPTER 6

EXPERIMENTAL METHOD

6.1. Materials

The Al_2O_3 - SiO_2 system is probably the most important in ceramic technology due to the abundance and wide spread use of alumina, silica, and alumina-silicate materials. Mullite, the only intermediate compound stable at high temperatures and normal pressures, is a commonly occurring phase in refractories, whitewares, and porcelains. Recent studies, with single crystal and high purity, high density polycrystalline mullite, have shown that only a fraction of mullite's potential capabilities, in regards to mechanical strength, creep resistance, and acid corrosion resistance are achieved in normal processing.¹⁻⁶ Potential applications of improved mullite-containing ceramics are refractory materials for coal gasifiers vessels,^{6,7} random materials,⁸ and high temperature structural materials.

Many methods have been used in forming mullite, from high temperature decomposition of naturally occurring alumino-silicates (such as clay minerals) to chemical preparation techniques involving high purity raw materials. Several reviews of these methods are available,^{4,9,10} however, on the sintering behavior of mullite-containing materials.

Several studies have been made on the kinetics of hot pressing of mullite.^{2,11} Referring to Al_2O_3 - SiO_2 phase diagram (Figs. 6-1 and 6-2) we notice that mullite with 75 wt.% Al_2O_3 presumably has no glassy phase at grain boundaries. Thus this composition was chosen for the single phase microstructure. For a microstructure with a continuous film of

glassy phase and pre-existing cavities at grain boundaries, a composition with 71.8 wt.% Al_2O_3 (mullite) was chosen.

There is a wide selection of Al_2O_3 and SiO_2 available. The starting materials in this study were A-14* aluminum oxide (α -alumina) and silica flour[†] (α quartz) which had purities of 99.8% and 99.6% respectively. Semi-quantitative spectrographic analyses[§] (Table 6-1) shows that the major impurity in A-14 was SiO_2 and the major impurity in the silica flour was Al_2O_3 . Mixing and de-agglomeration were achieved by wet (isopropyl alcohol) milling in a teflon lined vibratory mill.^{||} After stir drying and screening (-120 mesh) mixtures were calcined at 1650°C for 48 hours to form mullite. Reaction is considered complete when no α - Al_2O_3 was detected in X-ray diffraction pattern.[¶]

After calcination, mixtures were subjected to coarse crushing in a mechanically operated mortar and pestle** and wet (isopropyl alcohol) vibratory milling. The grinding time was 3 hours. After stir drying and screening (-120 mesh) powders were calcined at 600°C for 1 hour to volatilize any organic contamination. Powders were labeled according to composition. X-ray diffraction and microscopy have shown the most significant contamination in processing to be α - Al_2O_3 introduced by impact collisions during milling (high density alumina grinding media^{††} were used).

*Alcoa, Aluminum Corp. of America, Bauxite, Arkansas

†Ottawa Silica Co., Ottawa, Illinois

§American Spectrographic Laboratories, Inc., San Francisco, California

||Sweco, Inc., Los Angeles California

¶Norelco Diffractometer, Philips Electronics Instruments, New York

**Pulverisite, Alfred Fintsch Co., Germany

††Norton, Co., Akron, Ohio

††Coors Porcelain Co., Golden, Colorado

Table 6-1. Spectrographic Analysis of Raw Materials**

	Alcoa A-14	Ottwa Flour
Al	Principal Constituent	0.2%
Si	0.035%	Principal Constituent
Na	0.02	0.02
Ca	0.02	0.02
Mg	0.001	0.035
K	0.5*	0.5*
Ti	0.005	0.025
Fe	0.03	0.05
Ga	0.01	----
Cu	0.001	0.001
Mn	0.001	0.001
Zr	0.01	0.003
Cr	0.001	0.001
Ba	----	0.004
Zn	----	----
B	0.01	0.01
Pb	----	0.005
Ni	----	0.001
Sr	----	0.005

The above are reported as oxides of the elements indicated.

*0.05% was detection limit

**American Spectrographic Laboratories, Inc. San Francisco, California

6.2. Vacuum Hot Pressing

Pressure sintering was performed for the case of single phase micro structure on small batches of pre-reacted mullite (75 Wt.% Al_2O_3) powder in a graphite die at temperature of 1550°C and 500 psi. The die had a 3" diameter bore and the plungers fit loosely to accommodate grafoil lining on the walls and plunger faces. After a powder charge was loaded and tamped, the assembly was cold pressed to an estimated density of 30% of theoretical. The die assembly as shown in Fig. 6-3 was heated at a rate of $400\text{--}500^\circ\text{C/hr}$ to 1500°C as read from the Pt-Pt10% Rh thermocouple within the die. Pressure was exerted by virtue of the vacuum of the furnace changer design such that the powder compact was always under a pressure of 15 psi. At 900°C , 250 psi were applied externally. The external pressure was doubled at 1300°C and maintained throughout the balance of the cycle until the die had reached room temperature. The coefficient of expansion of graphite exceed that of mullite causing a hoop stress on the hot pressed disc as it cooled. Maintaining the pressure during cooling assured the integrity of the piece. The temperature was held at 1550°C for 1 hour and then allowed to cool at 400°C/hr until 1000°C at which time the furnace was turned off. Throughout the experiment the ram motion, vacuum, and temperature were recorded. Afterwards the expansion/contraction, rate thereof, temperature and vacuum were plotted simultaneously against time. The hot pressed disc was removed from the die.

A transmission electron micrograph of mullite (75 wt.% Al_2O_3) is shown in Fig. 6-2 at a magnification of 28,000X. This figure shows equilibrium dihedral angles indicating the absence of a second phase

at grain boundaries. Scanning electron micrographs of same composition but with cavities present is shown in Fig. 6-4 a and b. To generate a microstructure with a continuous film of glassy phase at grain boundaries along with cavities, a pre-reacted powder with 71.8 wt.% Al_2O_3 and 28.2 wt.% SiO_2 was hot pressed as described above to a maximum temperature of 1500°C with 100 psi external pressure applied. This gave a disc of 3" diameter and 1/8" thickness. Transmission electron micrograph showing acute dihedral angles and glassy phase at grain boundaries is shown in Fig. 6-5(a) and scanning electron micrograph with cavities at grain boundaries is shown in Fig. 6-5(b). After hot pressing, the samples were cut using a diamond blade and heated to 900°C for 4 hours to oxidize any carbon picked up from dies during hot pressing and then ground to a final size of 6.5 by 0.8 by 0.25 cm with faces of the bars flat and parallel and parallel to within ± 0.002 cm. Such precision was necessary to obtain correct values of the elastic modulus. After testing these samples, they were heated to 1750°C for 6 hours in Brew* furnace and tested again.

6.3. Properties

X-ray diffraction was performed under the following conditions: Scanning conditions were 40 kV, 20 mA, $1^\circ/\text{min}$, 1/4/1 entrance to exit collimation, time constant 3.0 and range 3×10^3 cps. High intensity copper K X-rays were used. In the single phase microstructure, mullite was the only phase detected. In the microstructure with a continuous film of glassy phase mullite was the only phase detected. No quantitative measurements of peak intensities were made. The descriptive assess-

*Brew, Concord, New Hampshire

ment of intensities were based on visual comparison of the heights for the strongest peak for each case.

Ceramographic polishing procedure consisted of grinding on (1) 200, 30, 15 and 6 micron metal bond diamond wheels. This was followed by vibratory polishing* using slurries of 6,1 and 1/4 micro diamond paste[†] and oil. Samples were observed by scanning electron microscopy.[§] A light etch with diluted hydrofluoric acid solution for the case of sample with a continuous film of glassy phase and a thin (~200 Å) gold coating was sometimes needed to bring out features.

For the case of single phase microstructure, the polished samples for viewing by SEM were thermally etched (1350°C) in order to make the grain boundaries visible. Etching was followed by coating with a thin gold layer. In order to determine average grain size, photographs were placed underneath a transparent plastic sheet, on which parallel lines had been drawn. The grain size was obtained by counting the number of grain boundaries intercepting straight lines of known length. Corrections for the presence of porosity were made according to the method of Wurst and Nelson.¹² Magnification and statistical (multiplication by 1.56) corrections were also made. Results are given in Table 6-2. Fraction, F, of triple point containing these cavities were also determined for the two microstructures and is given in Table 6-2.

* FMC Corp., Syntron Div., Homer City, Pennsylvania

† Metadi Diamond Compound, Buehler Ltd., Evanston, Illinois

§ AMR 1000, Advanced Metals Research Co., Bedford, Massachusetts

Table 6-2. Physical properties of the two microstructures

Properties	Single phase microstructure	Continuous glassy phase
grain size (d) μm	2.5	2
a (μm)	0.4	0.3
F	0.5	0.4

6.4. Modulus of Elasticity Measurements

Simple elasticity theory assumes that the stresses and strains in structural members are uniquely related to one another through the proportionality constants called the elastic constants. If the elastic constants of the material are known, the strain components may be calculated from the stress components or vice versa. For most engineering work it is assumed that the material is elastically isotropic. It is then necessary to define only two elastic constants, one relating normal stresses and strains and one relating shear stresses and strains. One is known as Young's modulus of elasticity and the other as the shear modulus.

There are two methods of determining values of Young's modulus--static and dynamic. In general, the dynamic method is capable of giving precise values without destruction of specimen and is more convenient than the static method. In addition, particularly at elevated temperatures, the static method introduces "anelasticity" (dependence of elastic deformation on time) and thus gives 'relaxed' modulus of elasticity. On the other hand, an instantaneous deformation on application of stress

defines 'unrelaxed modulus of elasticity.' Various equations¹³⁻¹⁵ have been derived to express the vibration of a bar-shaped specimen, all of which are approximate, utilizing correction terms to account for the individual modes of the vibration. The Young's modulus can be obtained from the transverse fundamental frequency as follows¹⁶

$$E = 0.96478 \times 10^{-8} \frac{P}{b} \left(\frac{L}{a} \right)^3 F_1^2 \quad (6.1)$$

where E is the Young's modulus in kg.mm⁻², P is the weight of sample in gms, L is length (cm), b is width (cm) and 'a' is thickness (cm), F₁ is the fundamental transverse frequency. Greater accuracy in the calculation of E is obtained when effects of shape, size and Poissons ratio are taken into account. The elastic modulus was calculated from this value and the dimensions and mass of the specimen. Use of tables published by Hasselman¹⁷ considerably reduced the calculation time.

At an elevated temperature, the value of Young's modulus, E_t, can be calculated using E₀ at room temperature as reference and the resonant frequency at temperature, T, providing allowance is made for the thermal expansion of the material.¹⁸ Thus,

$$E_t = E_0 \left(\frac{f_t}{f_0} \right)^2 \left(\frac{1}{1 + \alpha \Delta T} \right) \quad (6.2)$$

where α is the thermal expansion coefficient and ΔT is the difference between temperature T and room temperature. The quantity α may be obtained by dilatometer. However, in most ceramic materials, the quantity can frequently be ignored because of its low value.

6.5. Internal Friction Measurements

The internal friction of a solid material usually refers to 'damping capacity' and is a measure of its rate of self-absorption of vibrational energy. This is essentially the conversion of the vibrational energy into heat and the subsequent loss of the heat. In vibratory motion, the damping is characterized by a decrease in amplitude with time for instantaneous shock vibration, the damping causes a limitation of the maximum amplitude. This effect is usually observed as the sharpness of the peak in a resonance curve for low-damping solid materials and the broadness of the peak for high-damping solid materials.

It is well recognized that a measurement of the internal friction is a more sensitive method of studying 'anelastic' behavior of materials than is the measure of elastic constants. Because of the anelastic behavior of materials, the applications of harmonic vibrations leads to a phase difference between stress and strain and, consequently, a loss of vibrational energy which results in damping of mechanical vibrations. Therefore by using different modes of vibrations, at low or high stress, changes in state or condition can be followed without destruction of specimen, or changing any of the variables of the system. Hence, it is possible to study, with a single specimen, phenomena of recrystallization, of phase changes, of structural changes, and of other physical changes.

Several methods have been utilized by various investigators which are briefly reviewed below:

- Method 1: When the damping capacity of a material is sufficiently high to give a detectable hysteresis in plots of static stress-strain curves, the area of the hysteresis loop divided by the work of deformation is a measure of the corresponding internal friction.
- Method 2: Providing the damping of a material is sufficiently high to give a detectable variation, the material can be periodically stressed at constant maximum amplitude, when the rate of temperature rise or energy input is a measure of internal friction of the material.
- Method 3: When the damping is sufficiently high, say 10^{-2} or higher, measurement of heat loss under the steady state condition with periodic stressing can be correlated to internal friction.
- Method 4: When the damping is sufficiently high, the energy required to sustain a periodic vibration may be measured and used as a measure of internal friction. The greatest difficulty experienced in this method will be losses in the electrical system due to the electronic hysteresis.
- Method 5: When the damping is sufficiently high, a lateral deflection of a rotating shaft having a fixed mass at one end has been used as a measure of the internal friction.

Method 6: When a known torque is applied to the specimen and then released suddenly, a measure of the rate of amplitude decay of free vibrations can be used to measure internal friction. High stresses may be easily attained by this method, but low stress measurements are difficult to detect and record. During these measurements, changes in the state of material may be followed (due to the high stress). With an appropriate means for measuring the rate of decay, either high or low damping materials may be studied.

Method 7: Under a continuous vibrational process, where a specimen is freely suspended at either end near the node of the vibration, a measure of variation in amplitude of forced vibrations as the frequency is varied about a resonant frequency, can be used to determine internal friction. This is known as the resonance method and recently became popular with many investigators in the general field of solid state and particularly for ceramics.

In the present investigation, the resonance method was selected because this method provides (a) direct means of measuring the damping capacity, and (b) wide range measurements of the damping capacity up to fairly high temperatures (about 1200°C).

Internal friction measurements can be made by interrupting the excitation to the sample and counting the number of cycles it takes for the amplitude of oscillations of the sample to decay from a reference amplitude to $1/e$ of this amplitude. In our case, internal friction

was measured by 'width at half maximum' of the resonance curve. The value was obtained by locating the resonant frequency (at maximum amplitude) and then locating the two frequencies above and below the resonant frequency at which the amplitude decreased to half of the resonance amplitude. Internal friction is then obtained from the difference of the two frequencies and the resonant frequency by¹⁶

$$Q^{-1} = 1.8136 * \frac{F}{F_0} \quad (6.3)$$

In the dynamic measurement of Young's modulus and internal friction, the specimen is part of the vibrating system. Young's modulus was obtained using a sonic method pioneered by Forster¹⁹ and further explained by Spinner and Tefft.²⁰ A block diagram of the apparatus* is shown in Fig. 6-6. Such a system has a measuring range from 600 to 25,000 Hz, and provides for the standard off-the-shelf components. The system consists of (1) a driving circuit, (2) a pickup circuit, and (3) specimen support. In the driven excitation mode, the variable frequency oscillator supplies a driving voltage to the sending transducer. The transducer converts the electrical oscillations into mechanical oscillations and couples them to the sample. At the other end the mechanical vibrations of the sample are converted to electrical signals by the receiving transducer. These electrical signals are amplified and their amplitude is indicated on the meter and displayed on the oscilloscope screen.

The amplified signal is also applied to the counter unit which counts the frequency. If the signal is too weak to operate the counter

*Institut Dr. Förster, Rutlingen, Germany

unit, there is provision to connect the counter unit directly to the variable frequency oscillator instead of the amplifier. In this case the counter counts the number of cycles per second of the oscillator directly. In the self-excitation system, the feed back amplifier in connection with the sample and transducers forms an oscillator circuit. The frequency of oscillations is determined by the resonant frequency of the sample. The receiving transducer is connected to a second amplifier which feeds the signal into the metering circuit and the oscilloscope circuit. The frequency counter counts the number of cycles per second of the frequency. A disadvantage of this method of excitation is that the frequencies excited will be those most suitable for the feedback conditions existing. It is, however, worthwhile to experiment with the coupling or the phase adjustment to get proper excitation. Once this correct adjustment is found, very exact and convenient measurements are possible which do not require frequency or amplitude readjustments, even in cases where considerable changes in moduli or damping occur.

6.5a. Identification of the Vibrating Mode

As described previously, there are three types of vibrations normally excited, namely, flexural, torsional, and longitudinal. Besides, a rectangular bar has two types for any mode of flexural vibration, depending upon the relation of the direction of vibration to either cross sectional dimension. If the vibration is parallel to the short side of the cross section, it is generally called 'flatwise' flexural vibration; and if it is parallel to the long side of the cross section, it is called 'edgewise' flexural vibration. In order to calculate the

elastic moduli of the specimen, one must know exactly the type and mode of the vibration.

As the scanning frequency approaches the resonance frequency of the specimen, a Lissajous pattern appears on the oscilloscope. The frequency at which the maximum amplitude is observed is the resonance frequency. Since the Lissajous pattern, whose shape is controlled by the phase shift of the electronic signal, is an exact reflection of the mechanical vibration, it is possible to determine whether the motion of the specimen at the position of the driver and the pickup is of the same phase or opposite. When the Lissajous pattern is adjusted so that the direction of the diagonal is down to the left for the same phase, there will be no pattern at the nodes and a down-to-the right direction will occur for the opposite phase, as shown in Fig. 6-7.

By counting the number of nodes along the bar, one can determine the mode of vibration. Torsional modes gave the change in pattern along the cross-sectional face of the bar, as shown in Fig. 6-7. Except for some specimens which have an unusually low shear modulus, the fundamental torsional resonant frequency for thin rods or bars is higher than the fundamental flexural resonant frequency. The fundamental flexural vibration has two modes. The fundamental torsional vibration has only one node at the center. If one observes a resonant condition which has a node at the center, after observing the resonant condition with two nodes, one can anticipate that it is the torsional vibration.

An alternative approach is to identify the mode of vibration from the position of the nodes. Torsional vibrations give the same nodal position; the fundamental having a node at the center, and the first

overtone at 0.251 and 0.751 from one end of the specimen. Flexural vibrations give slightly different nodal positions, which are 0.2241 and 0.7761 for the fundamental mode. These nodal points can be made visible by placing a fine substance such as SiC powder on the specimen, as suggested by Hasselman;¹⁷ the grains will then accumulate at the position of the node. Measurements of internal friction with the Forster-type apparatus are complicated by energy loss and by resonances in the apparatus. At room temperature, the energy loss can be minimized and the true value of the internal friction can be determined. It is very laborious to make measurements at elevated temperatures because the internal friction of polycrystalline refractory oxides characteristically increases with increasing temperature to the point that the electrical noise level caused by resonances in the supporting wires is comparable to the amplitude of vibration of the specimen. For these measurements, particular precautions must be exercised, a few of which are as follows:

- 1) The size of suspension wires is critical. This is because the suspension wires themselves may sometimes be in resonance at some frequency near the resonant frequency of the specimen. This precaution requires special attention at elevated temperatures where energy losses of specimen become greater. The best solution is by trial and error, using different sizes and types of wires.

- 2) At elevated temperatures, the oxidation characteristics of the suspension wires demand consideration. When the oxidation reaction takes place on the wires, this seems to create excessive noises, possibly due to the effect of energy dissipation around the wires, which is difficult to separate from the noise of mechanical origin.

Forster in his original paper²¹ showed that with light specimens, it is necessary to keep the suspension near the nodes (suspension wires are also used for excitation and as vibration probe) of the sample or values of Q^{-1} much higher than true values may be obtained because of damping by suspension. Especially for low values of Q^{-1} , the effect of damping by suspension is very important; values of Q^{-1} in error by an order of magnitude may be obtained if this damping is not eliminated.²² The suspension damping can be reduced by moving the suspension near the nodes, but the suspension must be some distance away from the nodes in order to function as driver and as pickup. The practical question is as to whether both requirements can be satisfied at once, i.e. whether the suspension can be far enough from the nodes to permit effective driving and pickup and yet close enough to reduce support damping to an appreciable level. Thus a method of measuring specimen vibration which would be free from this difficulty was sought at kilo hertz frequencies.

6.5b. Suspension System

To avoid the above mentioned difficulties the specimen rested exactly at nodes on alumina rods and the sample was coupled to transducers by Pt + 40 wt.% wire (0.005" diameter) at the ends by drilling holes at diagonally opposite corners and using alumina cement. This means of coupling has the advantage that excitation of all three modes of vibration, transverse, torsional and longitudinal, and their respective harmonics are possible. The suitable placement of the wire contact will always produce a component to produce the desired mode of excitation. It also gives sufficient mechanical decoupling between the test rod and transducer to eliminate additional damping during

internal friction measurements. The disadvantage of the wire coupled system is that the degree of coupling is not defined. It is a function of wire direction and tension and in case of very unfavorable conditions, a function of the amplitude of vibration.

6.5c. Transducers

The conversion of electrical into mechanical energy is accomplished by transducers. Piezoelectric transducers undergo phase transformation and/or loose water of crystallization with temperature. Electrostatic transducers pick up induced field from furnace heating elements, etc. and electromagnetic transducers were used for ceramic samples after some modification. The electromagnetic field acts on a thin membrane consisting of 0.005" steel shim stock. A wire of 0.005" diameter constituting of Pt with 40 wt.% Rh, is spot welded at the center of the membrane. This wire transmits vibration to and from sample for driver and pickup transducers respectively.

The electromagnetic transducers contain a permanent magnet which produces a magnetic D.C. field in a yoke. An A.C. field of suitable frequency is superimposed into the D.C. field. The vibrating force on the membrane will be proportional to this field as long as this peak to peak value does not exceed the D.C. field. When the excitation and resonance frequency coincide, the specimen will oscillate. At the pickup transducer, the coupling wire vibrates the shim stock. As the distance between the shim stock and transducer varies during vibrations of the specimen, a voltage is induced in the windings which is of equal frequency. In order that direct electromagnetic coupling between the transducers may be avoided, the laminations of each transducers must be

3. Minimizing noises due to acoustic and static radiations which usually originate from the heating elements used. In this respect resistance heating elements rather than induction type are desirable and were used.

To meet the above specifications, a vertically split two piece furnace was used for the investigation of specimens at temperatures up to 1200°C as shown in Fig. 6-8. The furnace was constructed such that the electrical heating elements in the two positions completely surrounded the test compartment. The sample rests on two small alumina rods mounted on two D-shaped alumina supports which can be adjusted to place sample at nodes. The assembly is so chosen that the center of the sample coincides with the center of the furnace. As described earlier, electromagnetic transducers are used in conjunction with a special ferro-magnetic disc mounted on transducers. This disc rotates and the vibrations are conveyed to sample and vice-versa (receiver) through excitation wires (Pt + 40 wt.% Rh and 0.005" diameter) spot welded to center of these discs. Nonmagnetic spacers are used to adjust distance of the disc from electromagnetic transducers. At the beginning of high temperature experiments, the transducer mounting device should be adjusted so that the thermal expansion of the sample can be compensated by means of fine adjustment screws. The adjustment screws are first completely turned in, then as the temperature increases, the couplings are slightly tightened from time to time. In this manner an optimum condition of energy transfer is maintained. This operation is reversed when the temperature decreases to compensate for thermal contraction. The temperature was controlled using a Pt + 10 wt.% Rh

positioned so they are mutually perpendicular. Further all electrical leads should be well coiled to avoid extraneous electric/magnetic field pickup by transducers.

The most favorable conditions are obtained when the coupling wires are slightly bowed and flexible when pressing against the test rod. The most suitable mechanical coupling can be selected with the aid of two fine adjustment screws (Fig. 6-8) after the resonant frequency or its vicinity has been arranged. In order to prevent the wires slipping from test rod, small holes are drilled at the two ends of the sample diagonally apart and coupling wire attached by means of alumina cement. These transducers are identical and can be interchanged. The following are the electrical characteristics of the transducers:

Copper resistance : 150 ohms

Inductance : 100 mH

Maximum current : 40 mA

6.5d. High Temperature Measurements

Measurements of elastic constants and internal friction by dynamic method, at elevated temperature requires means of:

1. Obtaining a known uniform temperature over the length of a specimen,
2. Controlling this temperature during the process of a measurement, and

thermocouple and is measured via another Pt + 10 wt.% Rh thermocouple placed in the center of the specimen chamber. This set up is equally good for any atmosphere including vacuum.

A linear temperature dependence has been observed²³ for Young's modulus of several polycrystalline refractory oxides including aluminum oxide, magnesium oxide and thorium oxide above room temperature with the exception of a rapid reduction from linearity occurring at high temperatures. In Figs. 6-9, 6-11, 6-13 and 6-14, and Tables 6-3 to 6-8, the initial linear decrease in modulus above room temperature is due to thermal vibrational energy increasing the separation between atoms and slightly decreasing the force necessary for further separation. For a given frequency, a temperature will be reached where grain boundaries start becoming mobile resulting in relaxation of shear stresses acting on grain boundaries, and the elastic modulus will start decreasing rapidly. Beyond the temperature (T_p), corresponding to the peak in internal friction, Q^{-1} vs temperature (Fig. 6-10), the boundaries become sufficiently mobile and the shear stress along the grain boundaries is essentially relaxed at all times. Thus the rapid drop stops, whereas the linear drop due to thermal vibrational energy continues.

The drop in elastic modulus M , due to anelastic relaxation only (grain boundary relaxation) is given by²⁴

$$M - M_r = \delta M \left(\frac{\omega^2 \tau^2}{1 + \omega^2 \tau^2} \right) \quad (6.4)$$

Where M is elastic modulus, M_r is relaxed elastic modulus, δM is relaxation of the modulus, ω is frequency and τ is relaxation time.

Table 6-3. Data on commercial Al_2O_3 (3.599 g.cm^{-3} , 4200 c/s)

$T^{\circ}\text{C}$	$E \cdot 10^{-3} \text{ Kg.mm}^{-2}$
97	29.91
399	28.92
576	28.37
649	28.41
698	27.77
788	27.52
901	27.41

Table 6-4. Data for $\text{Al}_2\text{O}_3 + 1.5 \text{ wt.}\% \text{SiO}_2$

$T^{\circ}\text{C}$	$E \cdot 10^{-3} \text{ Kg. mm}^{-2}$	$f_r (\text{c/s})$	$\Delta f_r (\text{c/s})$	$Q^{-1} \cdot 10^3$
24	26.21	5076	2.88	1.028
500	24.85	4941	3.06	1.124
550	24.56	4912	3.09	1.141
681	24.35	4891	3.56	1.321
693	24.12	4868	3.62	1.349
711	24.16	4872	4.19	1.561
723	24.11	4867	4.76	1.774
734	24.06	4862	4.86	1.813
742	24.01	4857	4.75	1.773
747	23.89	4845	4.67	1.748
756	23.82	4838	4.59	1.721
762	23.78	4834	4.13	1.549
777	23.71	4827	4.12	1.547
787	23.76	4827	3.93	1.474
795	23.47	4830	3.95	1.483
831	23.64	4819	3.80	1.431
972	23.21	4775	6.06	2.301
1009	23.01	4755	6.88	2.623
1012	22.96	4750	6.81	2.601
1016	23.06	4760	7.55	2.876
1040	22.97	4751	8.65	3.301

Table 6-5. Data on 97.5 wt.% Al_2O_3 + 2.5 wt.% SiO_2

$T^{\circ}\text{C}$	$E \cdot 10^{-3} \text{ Kg. mm}^{-2}$
373	22.00
473	21.65
571	21.30
606	21.17
773	20.60
871	20.29
923	20.06
953	19.96
969	19.88
981	19.77
988	19.66
996	19.65
1009	19.63

Table 6-6. Data on 71.8 wt.% Al_2O_3 sample (mullite, porosity = 32%)

$T^{\circ}\text{C}$	$f_r(\text{c/s})$	$E \cdot 10^{-10}(\text{N/m}^2)$	$\Delta f_r(\text{c/s})$	$Q^{-1} \cdot 10^4$
241	14,560	13.69	2.52	3.14
317	14,501	13.58	2.48	3.10
439	14,437	13.46	2.53	3.18
667	14,265	13.14	3.00	3.81
682	14,232	13.08	3.17	4.04
711	14,210	13.04	3.31	4.22
722	14,199	13.02	3.47	4.43
729	14,205	13.03	3.74	4.77
737	14,177	12.98	3.65	4.29
744	14,156	12.94	3.89	4.98
753 (T_p)	14,166	12.96	3.94	5.04
772	14,128	12.89	3.52	4.52
780	14,079	12.80	3.81	4.91
813	14,035	12.72	3.23	4.17
827	14,013	12.68	3.43	4.44
850	13,890	12.46	3.48	4.54
872	13,829	12.35	4.00	5.25

Table 6-7. Data on mullite (75 wt.% Al_2O_3 , porosity = 28%)

$T^\circ\text{C}$	$f_r(\text{c/s})$	$E \cdot 10^{-10}(\text{N/m}^2)$	$\Delta f_r(\text{c/s})$	$Q^{-1} \cdot 10^4$
192	16,157	15.93	---	---
704	15,829	15.29	---	---
751	15,803	15.24	2.08	2.39
796	15,798	15.23	2.09	2.40
817	15,783	15.20	2.10	2.41
834	15,772	15.18	2.11	2.43
850	15,741	15.12	2.18	2.51
866	15,730	15.10	2.22	2.56
895	15,715	15.07	2.35	2.71
909	15,678	15.00	2.41	2.79
916 (T_p)	15,647	14.94	2.91	3.37
921	15,626	14.90	2.59	3.01
924	15,616	14.88	2.56	2.97
933	15,626	14.90	2.45	2.84
941	15,584	14.82	2.41	2.80
950	15,574	14.80	2.47	2.88
959	15,558	14.77	2.54	2.96
970	15,563	14.78	2.66	3.10
986	15,542	14.74	2.77	3.23
1044	15,489	14.64	---	---

Table 6-8. Data on 71.8 wt.% Al_2O_3 sample (mullite)

$T^{\circ}\text{C}$	f_r (c/s)	Δf_r (c/s)	$Q^{-1} \cdot 10^4$
217	4061	1.31	.584
476	3976	1.43	.650
608	3959	1.55	.709
647	3935	1.64	.755
665	3936	1.64	.754
703	3920	1.91	.882
731	3907	2.16	1.002
752 (T_p)	3903	2.39	1.110
768	3882	2.15	1.005
769	3874	1.94	.907
775	3868	1.97	.922
782	3872	1.87	.876
802	3858	1.96	.921
805	3850	2.03	.955
831	3843	2.10	.991
905	3800	3.19	1.523
958	3788	4.37	2.091
992	3762	5.17	2.492

By substituting $x = \ln \omega \tau$, Eq. (6.4) reduces to:

$$M - M_r = \frac{\delta M}{2} (1 + \tanh (S+U/T)) \quad (6.5)$$

Wachtman et. al.²⁵ have suggested an empirical expression for temperature dependence of elastic modulus for temperatures approaching absolute zero to sufficiently high temperatures before departure from linearity occurs in polycrystalline samples due to grain boundary slip.

$$M = M(0) - B \cdot T \cdot \exp(-T_0/T) \quad (6.6)$$

where $M(0)$ is value at absolute zero and is approached with zero slope as required by the third law of thermodynamics. At high temperatures $\exp(-T_0/T)$ approaches unity and the equation gives a linear dependence with temperature. This was given a theoretical basis by Anderson²⁶ in terms of a corresponding equation for bulk modulus. From Eq. (6.5) and (6.6), for polycrystalline materials above room temperature this can be described by:

$$M(T) = M(0) - C \cdot T - F(1 - \tanh (S+U/T)) \quad (6.7)$$

where $M(T)$ is the elastic modulus at temperature T K, $M(0)$ is the extrapolated value to 0 K of linear drop due to thermal vibrational energy, C is the slope of the linear decrease due to thermal vibrational energy, and F is the drop near T_p . For a material with single relaxation time (τ), $S = -U/T_p$ where U = Activation energy/gas constant. Though this equation is strictly true in the region of the internal friction peak and for a unique relaxation time, the form of the equation is also valid

for a distribution of relaxation times as shown in Fig. 6-12 and Table 6-5 for grain boundary relaxation in a specimen of Al_2O_3 with 2.5 wt.% SiO_2 . The rapid drop due to grain boundary sliding is quite significant. In the case of distribution of relaxation times the equation was fitted by adjusting the parameter U . This distribution of relaxation time occurs when only a fraction of the boundaries are in a condition to relax near T_p . Some already relax easily while others are still stiff. This is quite obvious from Fig. 6-12 and Table 7-1. A lognormal distribution in relaxation times was used to adequately describe the spectrum of relaxation times governing the grain boundary relaxation with distribution parameter of 3.25. A theoretical single relaxation time curve is also shown. An activation energy of 160 ± 20 Kcal/mole was found by peak shift due to change in frequency. This agrees well with literature values.²⁷⁻²⁹

Chang³⁰ in working with nominally pure polycrystalline Al_2O_3 found an internal friction peak at about 1100°C (~ 7 c/s). Wachtman³¹ found a peak at 1200°C (~ 1 Kc/s) whereas Crandall³² found a peak at 1080°C (~ 5 Kc/s). No special microstructural analysis was done concerning the microstructure of test specimens. Additions of small amounts of Cr_2O_3 or La_2O_3 gave rise to a peak around 850°C as found by Chang³⁰ who obtained an activation energy of 47 Kcal/mole for the peak due to Cr_2O_3 . He suggested that marked decrease in activation energy when small amounts of Cr_2O_3 was added can be understood by assuming that a smaller number of atoms are disordered during grain boundary slip when additives are present. The evidence, however, is not conclusive. Further, Chang suggested a new mechanism of grain boundary relaxation

based on creep and anelastic studies: a stress-induced formation, migration and annihilation of vacancies. At grain boundaries under tensile stress, vacancies (above equilibrium concentration) are formed. The activation energy of the process is the sum of that for formation and migration of a vacancy, which is the activation energy for self diffusion. When solute atoms are present, the activation energies for formation and migration of a vacancy near the solute atoms are markedly lowered. A new relaxation process involving the solute atom arises, presumable caused by stress induced formation, migration and annihilation of vacancy-solute aggregates near grain boundary. Further studies are required to verify the mechanism.

Further observations concerning the elastic behavior of polycrystalline materials have been made by Wachtman³³ and Ault³⁴. Again, in these investigations, no special comments were made concerning the microstructure of test specimens. Wachtman and Ault find non-linear decreases in elasticity of polycrystalline alumina from 600° to 900°C. Crandall also worked with $\text{Al}_2\text{O}_3 + 1 \text{ wt.}\% \text{SiO}_2$. According to Crandall et. al., X-ray examinations of all such samples revealed that mullite was formed with each addition of silica. One percent addition of silica produced 3% mullite; 3% silica addition produced 10% mullite; and 5% silica addition produced 17% mullite by weight. They found an internal friction peak around 700°C attributing it to the same phenomenon observed by Chang in Al_2O_3 with additions of Cr_2O_3 or La_2O_3 . Turnbough and Norton³⁵ found glassy phase in Wachtman³¹ and Chang³⁰ alumina samples and also in Chang's³⁰ $\text{Al}_2\text{O}_3\text{-Cr}_2\text{O}_3$ samples. They observed two relaxation mechanisms in alumina. Type I, a lower temperature relaxation, associated with a

peak, is impurity dependent. According to them a peak exists when the relaxation phenomena involves a back stress. On the other hand, Type II relaxation rises continuously without exhibiting a maximum and occurs at higher temperatures. According to them, it appears to stem from the intrinsic properties of grain boundaries as it was absent in single crystal Al_2O_3 even at temperatures where single crystal Al_2O_3 deformed visibly and was present in those polycrystalline specimens which contained no viscous phase. It was interpreted as arising from diffusion controlled grain boundary motion in Al_2O_3 .

An activation energy of 35 Kcal/mole was found to be associated with Type I relaxation in one of their Al_2O_3 sample which is within the range for viscous flow in silicate glasses. Chemical analysis of their alumina indicated the presence of impurities such as silica and alkali oxides. Impurity additions such as Cr_2O_3 and SiO_2 which should go into solid solution or form crystalline nonviscous phases respectively with the alumina at 1675°C for 3 hours do not appreciably alter Type II damping from that of pure alumina. According to them a small Type I peak in $\text{Al}_2\text{O}_3 + 1 \text{ wt.}\% \text{Cr}_2\text{O}_3$ is due to apparatus irregularities. It is to be noted that a viscous phase at grain boundaries is not just the result of impurities alone. In $\text{Al}_2\text{O}_3\text{-SiO}_2$ system, kinetic inaccessibility of formation of mullite makes metastability,³⁶⁻⁴² Fig. 6-1, realizable under normal experimental conditions. A sintering study⁴³ of mixed powders of alumina and silica show that formation of a viscous phase is a precursor to formation of mullite.

Alumina with 1.5 wt.% silica sample was hot pressed starting from appropriately mixed powders of alumina and quartz. The sample was hot pressed at 1550°C for one hour.

The initial drop in elastic modulus due to thermal vibrational energy is the same for commercial Al_2O_3 and $\text{Al}_2\text{O}_3 + 1.5 \text{ wt.}\% \text{ SiO}_2$ and can be explained by low solid solubility of SiO_2 in Al_2O_3 . In this temperature range grain boundaries are not mobile. Corresponding Q^{-1} vs temperature for $\text{Al}_2\text{O}_3 + 1.5 \text{ wt.}\% \text{ SiO}_2$ is shown in Fig. 6-10. The glass grain boundaries relax around 730°C which is close to glass transition temperature of alumino silicate glasses. The activation energy was found to be 45 ± 5 Kcal/mole. The activation energy matches well with literature values of activation energies obtained from bulk viscosity measurements.⁴⁴⁻⁴⁵

The drop in elastic modulus due to grain boundary sliding for 71.8 wt.% alumina and 28.2 wt.% SiO_2 sample having a continuous film of glassy phase at grain boundaries is shown in Fig. 6-13 and Table 6-6. Internal friction versus temperature plot is shown in Fig. 6-15 and Table 6-8. A corresponding drop in elastic modulus for 75 wt.% alumina and 25 wt.% silica sample is shown in Fig. 6-14 and Table 6-7. Internal friction versus temperature plot is shown in Fig. 7-1 and Table 7-1.

Thus dynamic elastic moduli and internal friction can be measured using electromagnetic transducers with special modification.

CHAPTER 7

RESULTS AND DISCUSSION

7.1. The Damping Spectra

The damping spectra for mullite (75 wt.% Al_2O_3) having single phase microstructure is shown in Fig. 7-1 and Table 7-1. Corresponding spectra for sample with glassy phase at grain boundaries (mullite 71.8 wt.% Al_2O_3) is shown in Fig. 6-15 and Table 6-6.

7.2. Comparison of Results with Theory

In order to determine if the mechanisms proposed for different microstructures are valid, experiments were conducted for the case of single phase microstructure and for the case of glassy phase at grain boundaries. The relaxation time τ for comparison with Eq. (5-1) for single phase microstructure and also for glassy phase microstructure was calculated from the condition $\omega\tau = 1$ where $\omega = 2\pi f$, is angular frequency of oscillation at the damping maximum. The normalization of the relaxation time for the variables of the experiment (excepting temperature) leads to Eq. (5.1) for the case of single phase microstructure and also for the case of microstructure with glassy phase at grain boundaries. Thus the theoretically calculated values are from the right hand side of the Eq. (5.1) for the two microstructures respectively. These are compared against experimental measurements of the left hand side of Eq. (5.1) corresponding to the two microstructures.

Table 7-1. Data on mullite (75 wt.% Al_2O_3)

$T^{\circ}\text{C}$	$f_r(\text{c/s})$	$\Delta f_r(\text{c/s})$	$Q^{-1} \cdot 10^3$	Q_{Norm}^{-1}
100	3543	4.44	2.302	
506	3472	4.57	2.416	
801	3420	4.68	2.511	0.119
817	3419	5.13	2.753	0.229
829	3410	6.28	3.383	0.370
852	3407	6.96	3.748	0.514
881	3405	9.23	4.975	0.950
897 (T_p)	3384	9.13	4.951	0.995
905	3383	7.00	3.801	
917	3374	4.52	2.461	
926	3373	4.43	2.461	0.817
941	3370	4.57	2.462	0.641
956	3364	4.57	2.463	0.400
988	3357	4.63	2.500	0.231
1018	3355	4.56	2.493	0.08
1035	3348	4.836	2.652	
1054	3345	5.20	2.854	
1097	3341	6.61	3.635	
1139	3327	9.50	5.178	
1172	3320	15.10	8.249	
1181	3319	19.17	10.475	

Normalized relaxation times for various tests are plotted logarithmically against reciprocal absolute temperature for single phase microstructure in Fig. 7-2 and Table 7-2 where it may be noted that the activation energy of 160 ± 20 Kcal/mole was obtained from the slope which matches well with literature values.¹⁻² Corresponding graphs of normalized relaxation times for various tests are plotted logarithmically against reciprocal absolute temperature for microstructures having continuous glassy film at grain boundaries in Fig. 7-3 and Table 7-3, where it may be noted that activation energy of 95 ± 5 Kcal/mole was obtained from the slope which matches well with literature values.³⁻⁴

Table 7-2. Internal friction data for sample with single phase microstructure ($\theta = 30^\circ$; $\kappa = 1.38$ corresponding to $a/l = 0.37$, $Q = 160 \pm 20$ Kcal/mole)

T (K)	f_r (c/s)	$\times 10^5$ s	$(\eta/\delta)_i \times 10^{-13}$ kg/m ² ·s	ln(L.H.S.) (Eq. 5.1)	ln(R.H.S.) (Eq. 5.1)
1145	1,156	13.77	11.53	4.56	5.31
1176	7,213	2.21	1.85	2.73	3.48
1190	15,650	1.02	0.85	1.96	2.71

Table 7-3. Internal friction data for sample having continuous glassy phase at grain boundaries ($\theta = 30^\circ$; $\kappa = 1.42$ corresponding to $a/l = 0.275$, $Q = 95 \pm 5$ Kcal/mole)

T(K)	f_r (c/s)	$\times 10^5 s$	$(\eta/\delta)_i \times 10^{-13} \text{ kg/m}^2 \cdot s$	$\ln(\text{L.H.S.})$ (Eq. 5.2)	$\ln(\text{R.H.S.})$ (Eq. 5.2)
986	2,109	7.55	5.24	4.18	4.60
1014	7,993	1.99	1.38	2.85	3.27
1026	14,166	1.12	0.78	2.27	2.70

The discrepancy between experimental data and theoretical prediction is partly due to using viscosity/unit thickness values for dense samples. Viscosity as well as effective grain boundary thickness might be different for cavitated and fully dense samples for the two microstructures under consideration. Further, not all grain boundaries relax at the same time and equiaxed grains are assumed in the analysis.

We interpret this to mean that grain boundary damping peaks observed in case of single phase microstructure and microstructure with glassy phase at grain boundaries result from grain boundary sliding accommodated by elastic deformation of the grains. The rate of sliding is controlled by grain boundary diffusion and cavities only play a small role in the accommodation process for the case of single phase microstructure as obvious from Fig. 2-3 and only $\sim 20^\circ\text{C}$ lowering in temperature due to the presence of cavities. Correspondingly the rate of sliding is controlled by viscous deformation (with no diffusion involved) and cavities also play only a minor role in the accommodation process for the case in which glassy phase is present at grain boundaries as obvious from Fig. 2-3 and

only $\sim 30^{\circ}\text{C}$ lowering in temperature due to presence of cavities. The activation energy did not change due to the presence of cavities which further indicates the small role played by cavities in the deformation process.

CHAPTER 8

HIGH TEMPERATURE BACKGROUND

8.1. Introduction

Zener¹ recognized, early, that thermal or atomic diffusion between grain boundaries, or near grain boundaries could contribute to damping. This results because thermoelastic differences between adjacent grains cause local stresses or strains near boundaries. These provide driving forces for redistribution of heat or solute atoms to new equilibrium configuration under load. However, because there are equilibrium end states, thermal or solute diffusion to grain boundaries will cause damping with distinct peaks; although as Zener¹ showed, they do not satisfy a simple Debye frequency relation. These losses are generally small compared to the sliding losses and predominant at different frequencies. Several other damping peaks caused by various solute diffusion mechanisms have been extensively investigated by De Batiste,² Nowick and Berry,³ but are generally not unique to polycrystalline materials and will not be considered here.

Later it was recognized by Friedel⁴ and Escaig⁵ that defect diffusion, that is, cyclic Nabarro-Herring creep, can also cause damping. For diffusion to and from boundaries there is no equilibrium end state and so background loss will increase without a limit at high temperature or low frequency. Diffusion can similarly cause cyclic dislocation climb; in principle, this can also increase without limit at low frequency, although at low stresses climb may be limited by the dislocation line tension giving a stress dependent limiting strain. Glide dislocations of course, also cause damping, but any slip involved in the high

temperature polycrystalline background is likely directly related to the stress concentrations at grain boundaries in contrast to the lower temperature peaks found in both single crystals and polycrystals. Gifkins⁶ and others have also suggested that diffusion at small ledges may be a limiting process in the sliding peak; however, depending upon the size of the steps, this process becomes indistinguishable from the background loss.

High temperature background has been analyzed here in terms of grain boundary diffusion in the transient case of non-uniform thickening of grain boundary.

8.2. Grain Boundary Sliding

When a remote stress σ_∞ is applied to a polycrystal, boundary sliding occurs with a relatively short relaxation time to generate stress singularities on adjacent boundaries (Fig. 8-1). The magnitude of singularities depends on the deformation properties of the material. For most polycrystalline ceramics, the grain can be assumed to respond in a linear viscous fashion. For this case, bounds on the singularity can be obtained from a two-dimensional solution with completely relaxed grain boundaries,⁷

$$\sigma \gtrsim 0.41 \sigma_\infty \sqrt{d/x} = K_u / \sqrt{x} \quad (8.1a)$$

where σ is the local stress, σ_∞ the remote stress, d the grain facet length and x the distance from the triple point; and from the solution for a single mode II penny crack⁸

$$\sigma \gtrsim 0.18 \sigma_\infty \sqrt{d/x} = K_L / \sqrt{x} \quad (8.1b)$$

These high local tensile stresses induce vacancy formation at boundary sources (to develop a vacancy supersaturation). The vacancies then diffuse to adjacent (compressively stressed) boundaries, and the stress singularity disappears, as indicated in Fig. 8-1. The relaxed stress distribution can be estimated by assuming that the time-dependent stress distribution $\sigma(x,t)$ has the form at $t = 0$ suggested by Eq. (8.1) and Fig. 8-2, viz:

$$\sigma(x,0) = \begin{cases} K/\sqrt{x} & x > 0 \\ -K/\sqrt{-x} & x < 0 \end{cases} \quad (8.2)$$

If $\delta = \delta(x,t)$ is the effective "thickening" of the grain boundary (due to the addition of matter to the crystals on each side), and J is the number of atoms diffusing along the grain boundary per unit time, per unit thickness into the plane of the diagram, mass conservation requires that

$$\Omega \partial J / \partial x + \partial \delta / \partial t = 0 \quad (8.3)$$

Further, the linearized law of diffusion is^{9,10}

$$\Omega J = - \frac{D_b \delta_b}{KT} \frac{\partial}{\partial x} (-\Omega \sigma) \quad (8.4)$$

where the equation has been arranged to emphasize that $-\Omega \sigma$ is the chemical potential per atom. Here $D_b \delta_b$ is the grain boundary diffusion parameter. Hence,

$$\frac{D_b \delta_b \Omega}{KT} \frac{\delta^2 \sigma}{\partial x^2} + \frac{\partial \delta}{\partial t} = 0 \quad (8.5)$$

A standard result of plane strain isotropic elasticity indicates that for a stress distribution

$$\sigma(x, t) = B(t) e^{-i\gamma x} \quad (8.6)$$

where B contains the time dependence of the stress acting along the axis. The required distribution of the "thickening" displacement is twice the surface displacement in the corresponding problem of load application to a half space. Thus e.g., following Chuang⁹ and Chuang et al.,¹¹

$$\delta(x, t) = - (2(1-\nu)/G\gamma)/B(t) e^{i\gamma x} \quad (8.7)$$

where G is the elastic shear modulus and ν in Poissons ratio. If the expressions for σ and δ are to satisfy the diffusion equation (3), it is necessary that

$$B(t) = B_0 \exp(-\alpha |\gamma|^3 t) \quad (8.8)$$

where

$$\alpha = \frac{G \delta_b D_b \Omega}{2(1-\nu)kT}$$

Hence if the initial stress distribution of Fig. 8-2 is represented by

$$\sigma(x, 0) = \int_{-\infty}^{\infty} B_0(\gamma) e^{i\gamma x} d\gamma \quad (8.10)$$

the stress distribution at any time $t > 0$ is

$$\sigma(x,t) = \int_{-\infty}^{\infty} B_o(\gamma) \exp(-\alpha|\gamma|^3 t) e^{i\gamma x} d\gamma \quad (8.11)$$

By Fourier inversion of Eq. (8.11) and a straight forward integration based on the form given earlier for $\sigma(x,0)$ gives the result

$$B_o(\gamma) = \frac{1}{2\pi} \int_{-\infty}^{\infty} \sigma(x,0) e^{-i\gamma x} dx \quad (8.12a)$$

$$= \frac{K}{2\pi} \left[- \int_0^{\infty} x'^{-1/2} e^{i\gamma x'} dx' + \int_0^{\infty} x^{-1/2} e^{-i\gamma x} dx \right] \quad (8.12b)$$

where $x' = -x$

$$= \begin{cases} -iK/2\sqrt{2\pi} |\gamma|^{1/2} & \gamma > 0 \\ iK/2\sqrt{2\pi} |\gamma|^{1/2} & \gamma < 0 \end{cases} \quad (8.12c)$$

where these results are inserted into the integral for $\sigma(x,t)$ (Eq. (8.11))

with $u^2 = \gamma x$ and $z = \alpha t/x^3$, the result is

$$\sigma(x,t) = \frac{K}{x^{1/2}} \cdot f(\alpha t/x^3) \quad (8.13)$$

where

$$f(z) = \frac{1}{\sqrt{2\pi}} \int_{-\infty}^{\infty} \exp(-zu^6) \sin u^2 du \quad (8.14)$$

which is plotted in Fig. 8-3 and can be represented as

$f(z) \approx 0.24 \exp(-0.095z)$. In case of internal friction $K = K_0 \cos \omega t$, then by standard superposition techniques

$$\sigma(x, t) = \int_{-\infty}^t \frac{dK(t')/dt'}{x^{1/2}} f\left(\frac{\alpha(t-t')}{x^3}\right) dt' \quad (8.15)$$

with $t'' = t - t'$, we get

$$\sigma(x, t) = -0.24\omega \int_0^{\infty} K_0 \frac{\sin(t-t'')}{x^{1/2}} \cdot \exp(-0.095\alpha t''/x^3) dt'' \quad (8.16)$$

with $q = \omega x^3/\alpha$ leads to

$$\sigma(x, t) = K_0 \left(\frac{\omega}{\alpha}\right)^{1/6} [\cos \omega t G(q) - \sin \omega t H(q)] \quad (8.17a)$$

where

$$G(q) = 0.24 \int_0^{\infty} q^{5/6} \cdot \sin qz \cdot \exp(-0.095z) dz \quad (8.17b)$$

$$= \frac{0.35 p^{11/6}}{1 + p^2} \quad (8.17c)$$

where $p \approx 10q$

and

$$H(q) = 0.24 \int_0^{\infty} q^{5/6} \cos qz \cdot \exp(-0.095z) dz \quad (8.17d)$$

$$= \frac{0.35 p^{5/6}}{1 + p^2} \quad (8.17e)$$

The average stress is obtained from

$$\sigma_{av} = \frac{2}{d} \int_0^{d/2} \sigma(x, t) dx \quad (8.18a)$$

and is

$$\sigma_{av} = 2 \frac{K_o}{d} \left(\frac{\omega}{\alpha} \right)^{1/6} \left[\cos \omega t \int_0^{d/2} G \left(\frac{\omega}{\alpha} x^3 \right) dx - \sin \omega t \int_0^{d/2} H \left(\frac{\omega}{\alpha} x^3 \right) dx \right] \quad (8.18b)$$

and internal friction Q^{-1} :

$$Q^{-1} = \frac{\int_0^{d/2} H \left(\frac{\omega}{\alpha} x^3 \right) dx}{\int_0^{d/2} G \left(\frac{\omega}{\alpha} x^3 \right) dx} \quad (8.19a)$$

$$= \frac{\int_0^{p^*} \frac{p^{1/6}}{1+p^2} dp}{\int_0^{p^*} \frac{p^{7/6}}{1+p^2} dp} \quad (8.19b)$$

where $p^* = \frac{5}{4} \frac{\omega}{\alpha} d^3$

(a) For $p^* < 1$, we get from Eq (8.19b)

$$Q^{-1} \approx \frac{13}{7p^*} \quad (8.20a)$$

which is the steady state result

(b) For $p^* > 1$, the integral in numerator of Eq. (8.19b) converges to ~ 1.4 and denominator to $6(p^*)^{-1/6}$

Thus

$$Q^{-1} \approx 0.24(p^*)^{-1/6} \quad (8.20b)$$

the transition from case (a) to (b) occurs $p^* \approx 10$

The results are plotted in Fig. 8-4 where contribution to high temperature background from diffusion accommodated grain boundary sliding (Eq. (8.20b)) and from diffusion at grain corners¹² is shown along with the total contribution to high temperature background internal friction which results from Eqs. (8.20a,b) and Ref. 12. Data for Al_2O_3 (Ref. 13) is also shown which matches well with the theory. The slight discrepancy

is due to grain size distribution and error in value of pre-exponential factor in diffusion data.¹⁴

Normalized stress distribution is shown in Fig. 8-5 (Appendix A) which shows that $x = 2.5(\alpha t)^{1/3}$ is a measure of the distance from the grain junction over which the stress concentration is seriously mitigated by diffusion. It is thus seen that the dimensionless parameter $(5(1-\nu^2) d^3 K T / E \Omega \delta_b D_b)$ is very suitable in representing data and future experimental data should be represented using this parameter.

CHAPTER 9

SUMMARY AND CONCLUSIONS

Grain boundary damping peaks in mullite (75 wt.% alumina) and a microstructure with 71.8 wt.% alumina and 28.2 wt.% SiO_2 with pre-existing cavities at grain boundaries were measured. The peaks were attributed to grain boundary sliding with elastic accommodation. It was thus concluded that:

1. Presence of pre-existing cavities had only a small contribution to the total grain boundary sliding.
2. The relaxation time for sliding varies with cavity size, cavity spacing and with grain size in accordance with models developed for the two microstructures.
3. The activation energy of the relaxation is in agreement with that for boundary diffusion in case of mullite with single phase microstructure.
4. The activation energy of the relaxation is in agreement with that of viscous flow in case of microstructure with a glassy phase at the grain boundaries with cavities behaving as shear cracks under grain boundary sliding.
5. The transient case for high temperature background was solved and it was well represented by a dimensionless parameter which was a function of frequency, grain size, elastic modulus and grain boundary diffusivity.

It is further concluded that internal friction measurements provide a useful method for measuring rates of grain boundary sliding with elastic accommodation.

APPENDIX A

RELAXED STRESS DISTRIBUTION

When Eq. (8.12c) is inserted in Eq. (8.11) and $Y = v^2/(\alpha t)^{1/3}$ is substituted, the result is

$$\sigma(x, t) = \frac{K}{(\alpha t)^{1/6}} \cdot H \frac{x}{(\alpha t)^{1/3}} \quad (H.1)$$

where

$$H(Y) = \sqrt{\frac{2}{\pi}} \int_{-\infty}^{\infty} \exp(-v^6) \cdot \sin(v^2 \cdot Y) dv \quad (H.2)$$

where

$$Y = x/(\alpha t)^{1/3} \quad (H.3)$$

A plot of normalized stress distribution is shown in Fig. 8-5, which depicts a maximum at $x = 2.5(\alpha t)^{1/3}$, which is a measure of the distance from the grain junction over which the stress concentration is seriously mitigated by diffusion.

REFERENCES

Chapter 2

1. R. C. Folweiler, Jnl. Appl. Phys., 32, 773 (1961).
2. N. J. Tighe, Jnl. Mater. Sci., 13, 1455 (1978).
3. T. J. Chuang and J. R. Rice, Acta Met., 21, 1625 (1973).
4. V. Vitek, Acta Met., 26, 1345 (1978).
5. M. V. Speight, W. B. Beere and G. Roberts, Mat. Sci. Eng., 36, 155 (1978).
6. T. J. Chuang, K. I. Kagawa, J. R. Rice and L. B. Sills, Acta Met., 27, 265 (1979).
7. R. Raj and M. F. Ashby, Acta Met., 23, 653 (1975).
8. R. Raj and C. H. Dang, Phil. Mag., 32, 909 (1975).
9. A. G. Evans and A. Rana, Acta Met., 28, 129 (1980).
10. A. N. Stroh, Advances in Physics, 6, 418 (1957).
11. A. H. Cottrell, Trans. AIME, 212, 197 (1958).
12. S. N. Chatterjee, Int'l Jnl. Solid Structures, 11, 521 (1975).
13. B. A. Bilby and J. D. Eshlby, Fracture, ed., H. Liebowitz, Academic Press, Vol. 1, 101 p. (1968).

Chapter 4

1. D. Hull and D. Rimmer, Phil. Mag., 4, 673 (1959).
2. R. W. Balluffi and L. L. Seigle, Acta Met., 5, 449 (1957).
3. R. C. Gifkins, Acta Met., 4, 98 (1956).
4. C. W. Chen and E. S. Machlin, Acta Met., 4, 655 (1956).
5. Y. Ishida and D. Mclean, Met. Sci. J., 1, 171 (1967).

6. P. Bowring, P. W. Davies, and B. Wilshire, *Met. Sci. J.*, 2, 168 (1968).
7. P. W. Davies and R. Dutton, *Acta Met.*, 14, 1138 (1966).
8. P. W. Davies and K. R. Williams, *Met. Sci. J.*, 3, 220 (1969);
ibid., 3, 48 (1969).
9. R. T. Ratcliffe and G. W. Greenwood, *Phil. Mag.*, 12, 59 (1965).
10. H. E. Evans, *Phil. Mag.*, 23, 1101 (1971).
11. A. H. Cottrell, *Trans., Metall. Soc. AIME.*, 212, 192 (1961);
Structural Processes in Creep, London: Iron and Steel Institute,
p. 5.
12. J. J. Gilman, *Trans. Met. Soc. AIME.*, 212, 783 (1967).
13. J. A. Williams, *Phil. Mag.*, 15 (1), 1289 (1967).
14. R. C. Gifkins, 'Fracture', Butterworths, London, p. 44-60 (1963).
15. B. J. Nield and A. G. Quarrell, *J. Inst. Met.*, 85, 480 (1956-57).
16. C. W. Chen and E. S. Machlin, *Acta Met.*, 6, 454 (1958).
17. D. Kramer and E. S. Machlin, *Acta Met.*, 6, 454 (1958).
18. P. W. Davies, T. C. Finnica and B. Wilshire, *J. Inst. Met.*, 90,
368 (1961-620).
19. *Idem*, *ibid.*, 91, 289 (1961-62).
20. J. Intrater and E. S. Machlin, *Acta Met.*, 7, 140 (1959).
21. J. H. Hensler and G. V. Cullen, *J. Australian Inst. Met.*, 9, 38
(1964).
22. P. W. Davies and J. P. Dennison, *J. Inst. Met.*, 88, 471 (1959-60).
23. A. Gittins, *Met. Sci. J.*, 4, 186 (1970).
24. T. Johannesson and A. Tholen, *J. Inst. Met.*, 97, 243 (1969).

25. I. J. Spark and D. M. R. Taplin, J. Australian Inst. Met., 14, 298 (1969).
26. P. W. Davies and K. R. Williams, Met. Sci. J., 4, 187 (1970).
27. R. V. Day, J. Iron Steel Inst., 203, 279 (1965).
28. A. Gittins and H. D. Williams, Phil. Mag. 16, 849 (1967).
29. D. M. R. Taplin, Phil. Mag. 20, 1079 (1969).
30. H. E. Evans, Met. Sci. J., 3, 33 (1969).
31. B. Wilshire, Scripta Met., 4, 361 (1970).
32. G. W. Greenwood, 'Interfaces', Butterworth, London, p. 223-235, (1969).
33. E. S. Machlin, 'Fracture', John Willey, N. Y., p. 45-46 (1959).
34. D. M. R. Taplin, Met. Eng. Quart., 10, 31 (1970).
35. B. Wilshire, "Practical Implications of Fracture Mechanisms," Met. Trust, London (1973).
36. J. W. Hancock, Metal Sci., Sept., 319 (1976).
37. T. J. Chuang and J. R. Rice, Acta Met., 21, 1625 (1973).
38. V. Vitek, Acta Met., 26, 1345 (1978).
39. M. V. Speight, W. B. Beere and G. Roberts, Mat. Sci. Eng., 36, 155 (1978).
40. T. J. Chuang, K. I. Kagawa, J. R. Rice and L. B. Sills, Acta Met., 27, 265 (1979).
41. J. A. Williams, Phil. Mag., 15, 1289 (1971).
42. H. E. Evans, Phil. Mag., 23, 945 (1971).
43. T. G. Langdon, Phil., Mag., 23, 945 (1971).
44. P. T. Heald and J. A. Williams, Phil. Mag., 24, 1215 (1972).
45. R. Raj and M. F. Ashby, Met. Trans., 2, 113 (1971).

46. L. K. V. Lou, T. E. Mitchell and A. H. Heuer, J. Am. Cer. Soc., 61, 392 (1978).
47. O. Krivanek, T. Shaw and G. Thomas, J. Am. Cer. Soc., in press.
48. Y. Ishida and M. Henderson Brown, Acta Met., 15, 857 (1967).

Chapter 6

1. P. C. Dokko, J. A. Pask and K. S. Mazdiasni, J. Am. Cer. Soc., 60, 150 (1977).
2. R. Penty, 'Pressure Sintering Kinetics and Mechanical Properties of High Purity Mullite,' Ph.D. thesis, Lehigh University, 1972.
3. K. S. Mazdiasni and L. M. Brown, J. Am. Cer. Soc., 58, 149 (1975).
4. M. D. Sacks, 'Correlation of Microstructure of Sintered Mullite Bodies with their Stress-Strain Behavior in Compression Loading at 1200°C, M. S. thesis, University of California, Berkeley (1971); and Lawrence Berkeley Laboratory Report, LBL-6205 (1971).
5. P. A. Lessing, R. S. Gordon and K. S. Mazdiasni, J. Am. Cer. Soc. 58, 149 (1975).
6. M. D. Sacks and J. A. Pask, 'Structure, Strength, and Corrosive Resistance of Alumino-Silicate Materials,' Dept. of Mat. Sci. and Min. Eng., University of California, Berkeley (1978).
7. J. A. Pask, R. B. Langston, S. T. Tso, and J. A. Pask, *ibid.* (1979).
8. G. S. Perry, Trans and J. Brit. Ceram. Soc., 72, 279 (1973).
9. J. Grofesik, 'Mullite, Its Structure, Formation and Significance, Publishing House of the Hungarian Academy of Sciences, Budapest (1961).

10. R. F. Davis and J. A. Pask, in: High Temperature Oxides, ed., A. M. Alper, Academic Press, N. Y., Vol. 4 (1971).
11. B. Ghate, 'Synthesis and Pressure Sintering Kinetics of High Purity Fine-Grained Mullite,' Ph.D. thesis, Lehigh University (1973).
12. J. C. Wurst and J. A. Nelson, J. Am. Cer. Soc., 55, 109 (1972).
13. G. Pickett, 'Equations for Computing Elastic Constants from Flexural and Torsional Resonant Frequencies of Vibration of Prisms and Cylinders', ASTM Proc., 45, 846-865 (1945).
14. N. P. Mason, 'Motion of Bar Vibrating in Flexure', J. Acoust. Soc., 8(4), 246-48 (1938).
15. Lord Rayleigh, 'Theory of Sound,' Vol. 1, Dover Publ. Co.
16. Operating Manual, Elastomat, Model type FM-500, Institut Dr. Forster, Reutlingen, West Germany.
17. D. P. H. Hasselman, 'Tables for Computation for the Shear Modulus and Young's Modulus of Elasticity from the Resonant Frequencies of Rectangular Prisms,' Carborundum Co., Niagara Falls, N.Y. (1961).
18. (a) N. N. Ault and H. G. Ueltz, 'Sonic Analysis for Solid Bodies,' J. Am. Cer. Soc., 36(6), 199-203 (1953).
(b) S. Spinner, 'Elastic Moduli of Glasses by a Dynamic Method,' J. Am. Cer. Soc., 37(5), 229-34 (1954).
19. Fritz Forster, 'New Method for the Determination of the Modulus of Elasticity and Damping,' Z. Metallk., 29(4), 116-23 (1937).
20. S. Spinner and W. E. Tefft, 'Method for Determining Mechanical Resonance Frequencies and for Calculating Elastic Moduli from these Frequencies,' ASTM Proc., 61, 1221-38 (1961).
21. F. Forster, Z. Metallk., 29, 109 (1937).

22. J. B. Wachtman, Jr. and W. E. Tefft, Rev., Sci. Instr., 29(6), 517 (1958).
23. J. B. Wachtman and D. G. Lam, J. Am. Cer. Soc., 42, 254 (1959).
24. A. S. Nowick and B. S. Berry, 'Anelastic Relaxation in Crystal-line Solids,' Academic Press, N. Y. (1972).
25. J. B. Wachtman, Jr., W. E. Tefft, D. G. Lam and C. S. Epstein, Phy. Rev., 122(6), 1754 (1961).
26. O. L. Anderson, Phy. Rev., 144(2), 553 (1966).
27. Ihlán Aksay, Ph.D. thesis, University of California, Berkeley (1973); and Lawrence Berkeley Laboratory Report, LBL-1403.
28. C. O. Hulse and Joseph A. Pask, J. Am. Cer. Soc., 49(6), 314 (1966).
29. R. A. Penty and D. P. H. Hasselman, Mat. Res. Bull., 7(10), 1117 (1972).
30. R. Chang, J. Nuc. Matls., 1(2), 174-81 (1959).
31. J. B. Wachtman, Jr. and L. H. Maxell, Tech. Rept. No. WADC-TR 57-526, Contract No. AF33(616) 56-4; 67 p., December 1957.
32. W. B. Crandall, D. H. Chung, and T. J. Gray, in: Mechanical Properties of Engineering Ceramics, ed., W. W. Kriegel and Hayne Palmour III, Interscience Publishers, Inc., N.Y. (1961).
33. J. B. Wachtman, Jr., and D. G. Lam, J. Am. Cer. Soc., 36, 199 (1953).
34. N. N. Ault and H. F. G. Ueltz, J. Am. Cer. Soc., 36, 199 (1953).
35. J. E. Turnbaugh and F. H. Norton, J. Am. Cer. Soc., 51(6), 344 (1968).
36. R. F. Davis and J. A. Pask, J. Am. Cer. Soc., 55, 525 (1972).
37. I. A. Aksay and J. A. Pask, ibid., 58, 507 (1975).

38. F. M. Wahl, R. E. Grim, and R. B. Graf., Amer. Mineral, 46, 1064 (1961).
39. W. G. Statley and G. W. Brindley, J. Am. Cer. Soc., 52, 616 (1969).
40. F. L. Kennard, R. C. Bradt, and V. S. Stubican, 'Reactivity of Solids, ed., J. S. Anderson, North Holland, Amsterdam, 580 (1972).
41. Dong-Hi Lee and R. McPherson, J. Matl. Sci., 15, 25 (1980).
42. R. McPherson, J. Am. Cer. Soc., 63, 110 (1980).
43. A. P. S. Rana and J. A. Pask, "Kinetics of Sub-Solidus Reactions in Al_2O_3 - SiO_2 ceramics," to be presented at 33rd Pacific Coast Regional Meeting of American Ceramic Society, Oct. 26-29, 1980.
44. R. Rossin, J. Bersan, and G. Urbain, Comptes Rendus Acad. Sc. Paris, 258(2), 562 (1964).
45. B. S. Mitin and Yu A. Nagibin, Izv. Vyssh. Uchleb. Zaved, Cern Met., 12(7), 8 (1969).

Chapter 7

1. R. A. Penty and D. P. H. Hasselman, Mater. Res. Bull., 7(10), 1117-24 (1972).
2. B. B. Ghate, Ph.D. thesis, Lehigh University, Bethelham, Pennsylvania (1971).
3. R. Rossin, J. Bersan and G. Urbain, Comptes Rendus Acad. Sc. Paris, 258(2), 562 (1964).
4. B. S. Mitin and Yu A. Nagibin, Izv. Vyssh. Uchleb. Zaved, Cern Met., 12(7), 8 (1969).

Chapter 8

1. C. Zener, 'Elasticity and Anelasticity of Metals, University of Chicago Press, Chicago, Chpt. 5 (1948).
2. De Batiste, J., Internal Friction of Structural Defects in Crystalline Solids, North-Holland Publishing Co., Amsterdam (1972).
3. A. S. Nowick and B. S. Berry, 'Anelastic Relaxation in Crystalline Solids, Academic Press, N. Y., Chpt. 15, p. 436 (1972).
4. J. Friedel, 'Fluage et Frottement Interieur de Haute Temperature,' Metaux et. Corrosion, 36, 148 (1961).
5. B. Escaig, 'Frottement Interieur de Haute Temperature at Diffusion de Lacunes Entre les Dislocations,' Acta Met., 10, 829 (1962).
6. R. C. Gifkins, 'Development on the Island Model for Grain Boundaries,' Mater. Sci. and Eng., 2, 181 (1967).
7. C. W. Lau and A. S. Argon, Fracture, ed., D. M. R. Taplin, University of Waterloo Press, 2, 595 (1977)
8. B. R. Lawn and T. R. Wilshaw, Fracture of Brittle Solids, Cambridge University Press (1976).
9. T. J. Chuang, 'Models of Intergranular Creep Crack Growth by Coupled Crack Surface and Grain Boundary Diffusion,' University of Microfilms Int. (Ann Arbor, Mich. Order No. 76 (56) 8, 95 pp: Diss. Abstr., Int. B. 37(1), 402 (1976).
10. R. Raj and M. F. Ashby, 'Grain Boundary Sliding and Diffusional Creep,' Metall. Trans., 2(4), 113-27 (1971).
11. T. J. Chuang, K. I. Kagawa, J. R. Rice and L. B. Sills, 'Non-equilibrium Models for Diffusive Cavitation of Grain Interfaces,' Acta Met., 27(3), 265-84 (1979).

12. Rowland M. Cannon, Ph.D. thesis, MIT, June 1975.
13. J. E. Turnbaugh and F. H. Norton, 'Low Frequency Grain Boundary Relaxation in Al_2O_3 , 51(6), 344 (1968).
14. R. M. Cannon and R. L. Coble, 'Review of Diffusional Creep in Al_2O_3 , in: Deformation of Ceramic Materials,' ed., R. C. Bradt and R. E. Tresler, Plenum Press, N. Y. (1975).

FIGURE CAPTIONS

- Fig. 2-1. The variations of stress intensity factor with crack length and angle for a kinked crack subject to in-plane shear and small closure tractions.
- Fig. 2-2. Variation of ratio of elastic displacement due triple point cavities to mode II shear displacement as a function of cavity size and angle.
- Fig. 6-1. The extensions of the SiO_2 and Al_2O_3 liquid to form the meta-stable phase diagram without mullite superimposed on the SiO_2 - Al_2O_3 equilibrium phase diagram.
- Fig. 6-2. Transmission electron micrograph of mullite (75 wt.% Al_2O_3) with equilibrium dihedral angles.
- Fig. 6-3. Cutaway view of hot pressing assembly. A-Pyrolytic graphite spacers, B-water cooled steel ram for pressure application (at top), C-graphite plunger, D-graphite die, E-powder charge, F-thermocouple in protection tube (G), H-furnace can, I-furnace lid lined with insulating felt, J-molybdenum mesh furnace element, K-connections to power leads.
- Fig. 6-4. Scanning Electron Micrographs of Mullite (87 wt.% Al_2O_3) with cavities at grain boundaries.
- Fig. 6-5. Electron micrograph of mullite (71.8 wt.% Al_2O_3).
(a) Transmitter electron micrograph showing acute dihedral angle and glassy phase. (b) Scanning electron micrograph showing cavities at grain boundaries.
- Fig. 6-6. Block diagram used for apparatus used for bar resonance.
- Fig. 6-7. The resonant vibrations in a rectangular bar.

Fig. 6-8. Furnace with transducer assembly. (1) Furnace, vertically split two piece, (2) Electro-magnetic transducers, (3) Ferro-magnetic vibrating thin disc, (4) Holder for disc, (5) Sample support, (6) Thermocouple, (7) Excitation wire, (8) Non-magnetic spacer.

Fig. 6-9. Temperature dependence of Young's modulus of elasticity for polycrystalline (a) commercial Al_2O_3 , (b) $\text{Al}_2\text{O}_3 + 1.5 \text{ wt.}\% \text{SiO}_2$.

Fig. 6-10. Internal friction as a function of temperature for polycrystalline $\text{Al}_2\text{O}_3 + 1.5 \text{ wt.}\% \text{SiO}_2$. Average surface area (μ^2/grain) = 25.

Fig. 6-11. Theoretical curve fitted to experimental data for $\text{Al}_2\text{O}_3 + 2.5 \text{ wt.}\% \text{SiO}_2$ sample.

Fig. 6-12. Normalized internal friction (with background subtracted) as a function of reciprocal absolute temperature for mullite (75 wt.% Al_2O_3). (a) Experimental curve with distribution parameter of 3.25. (b) Theoretical curve for single with distribution parameter of zero.

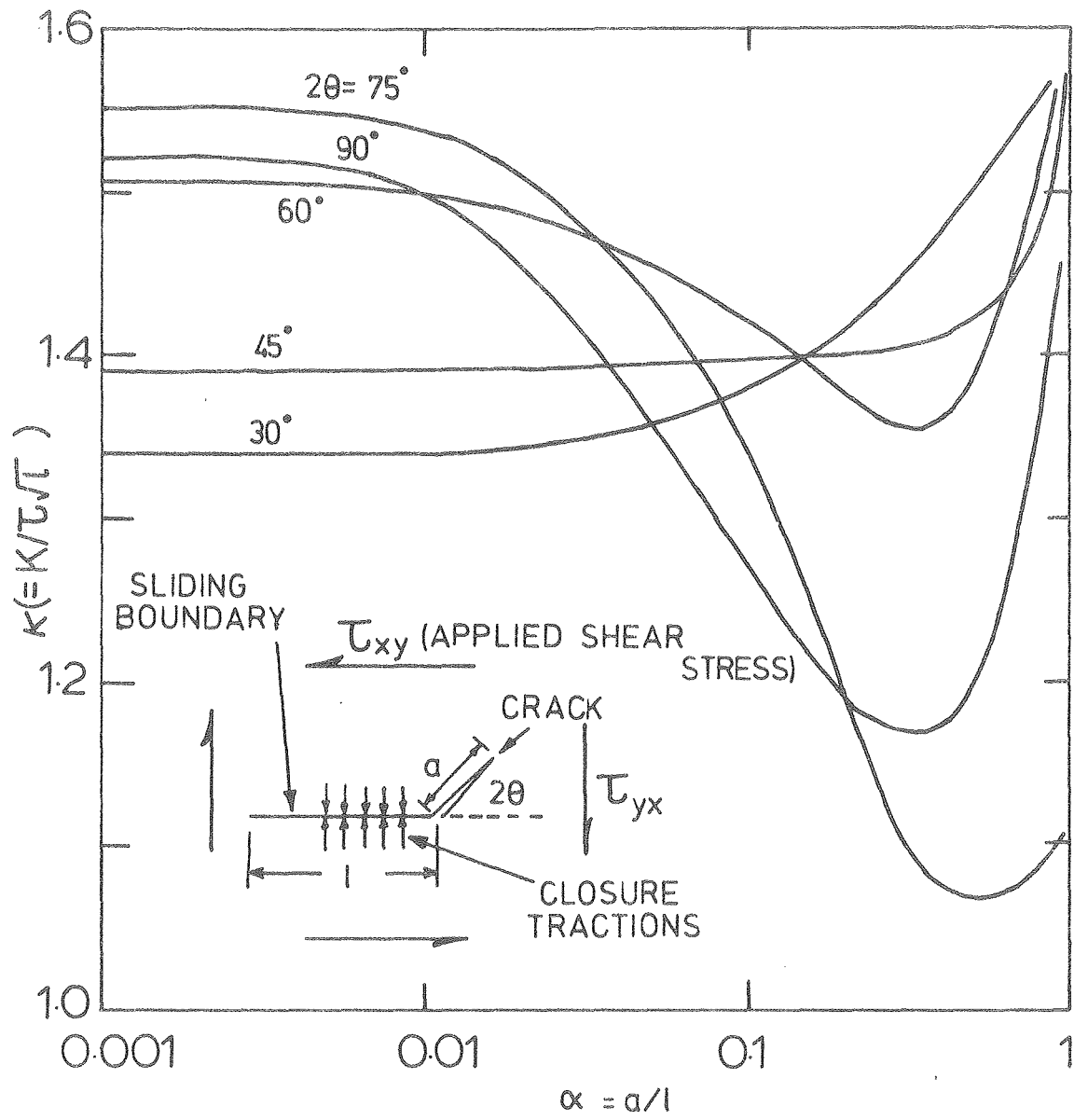
Fig. 6-13. Temperature dependence of Young's modulus of elasticity for mullite (71.8 wt.% Al_2O_3 , porosity $\approx 32\%$).

Fig. 6-14. Temperature dependence of elastic modulus of mullite (75 wt.% Al_2O_3 , porosity = 28%).

Fig. 6-15. Internal friction (Q^{-1}) vs temperature for mullite (71.8 wt.% Al_2O_3).

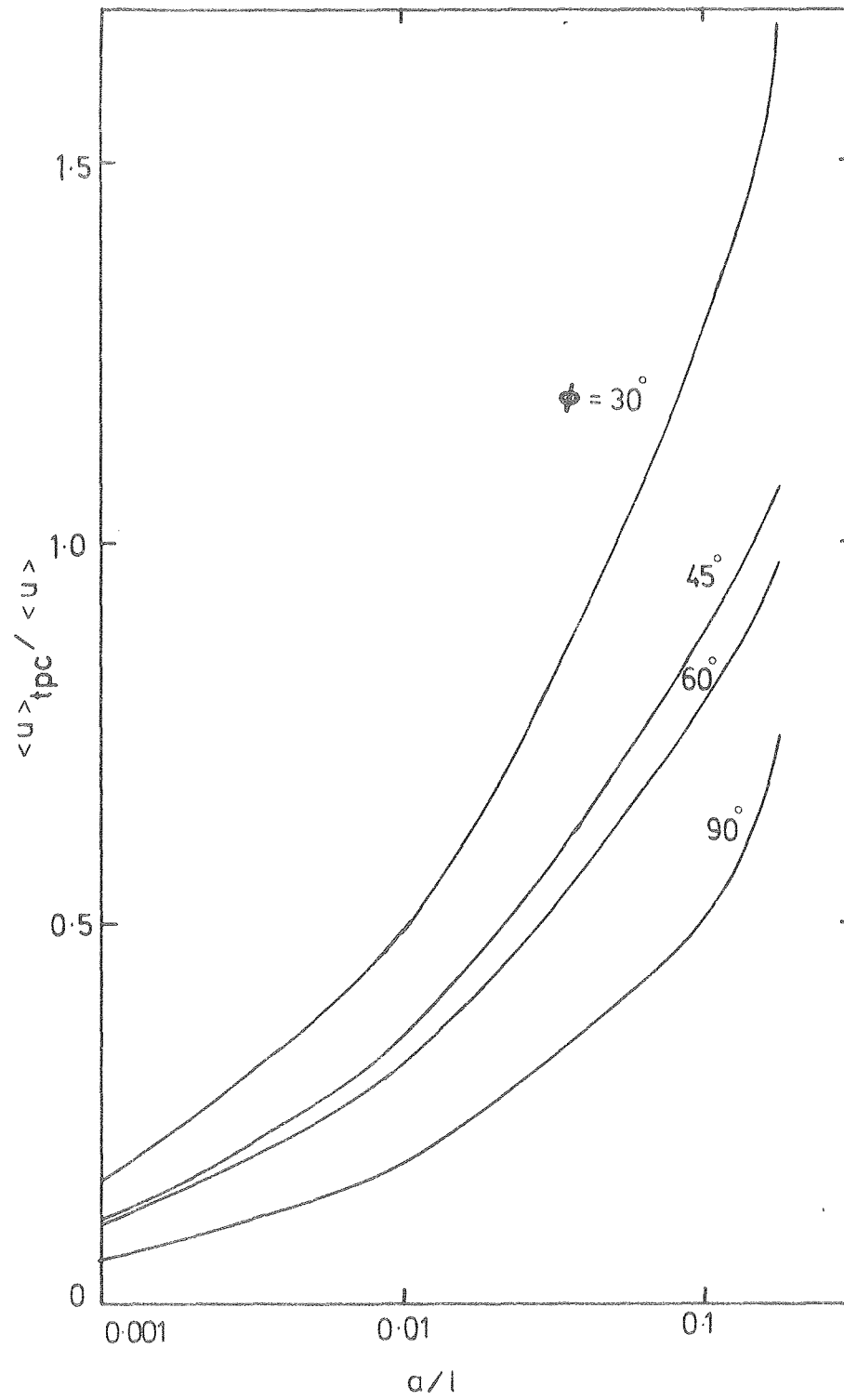
Fig. 7-1. Internal friction (Q^{-1}) vs temperature curve for mullite (75 wt.% Al_2O_3).

- Fig. 7-2. Normalized relaxation time plotted as a function of reciprocal absolute temperature for mullite (75 wt.% Al_2O_3).
- Fig. 7-3. Normalized relaxation time plotted as a function of reciprocal absolute temperature for mullite (71.8 wt.% Al_2O_3).
- Fig. 8-1. Stress developed ($x > 0$) as a result of freely sliding grain boundaries.
- Fig. 8-2. Initial stress distribution and its relaxation by diffusional accommodation.
- Fig. 8-3. Stress distribution plotted using normalized coordinates suggested by the analysis.
- Fig. 8-4. Contribution to high temperature background internal friction from diffusion accommodated grain boundary sliding and grain boundary diffusion. Data for Al_2O_3 is also shown.
- Fig. 8-5. Relaxed stress distribution plotted using normalized coordinates. $x = 2.5 (\alpha t)^{1/3}$ is the effective distance over which diffusion occurs.



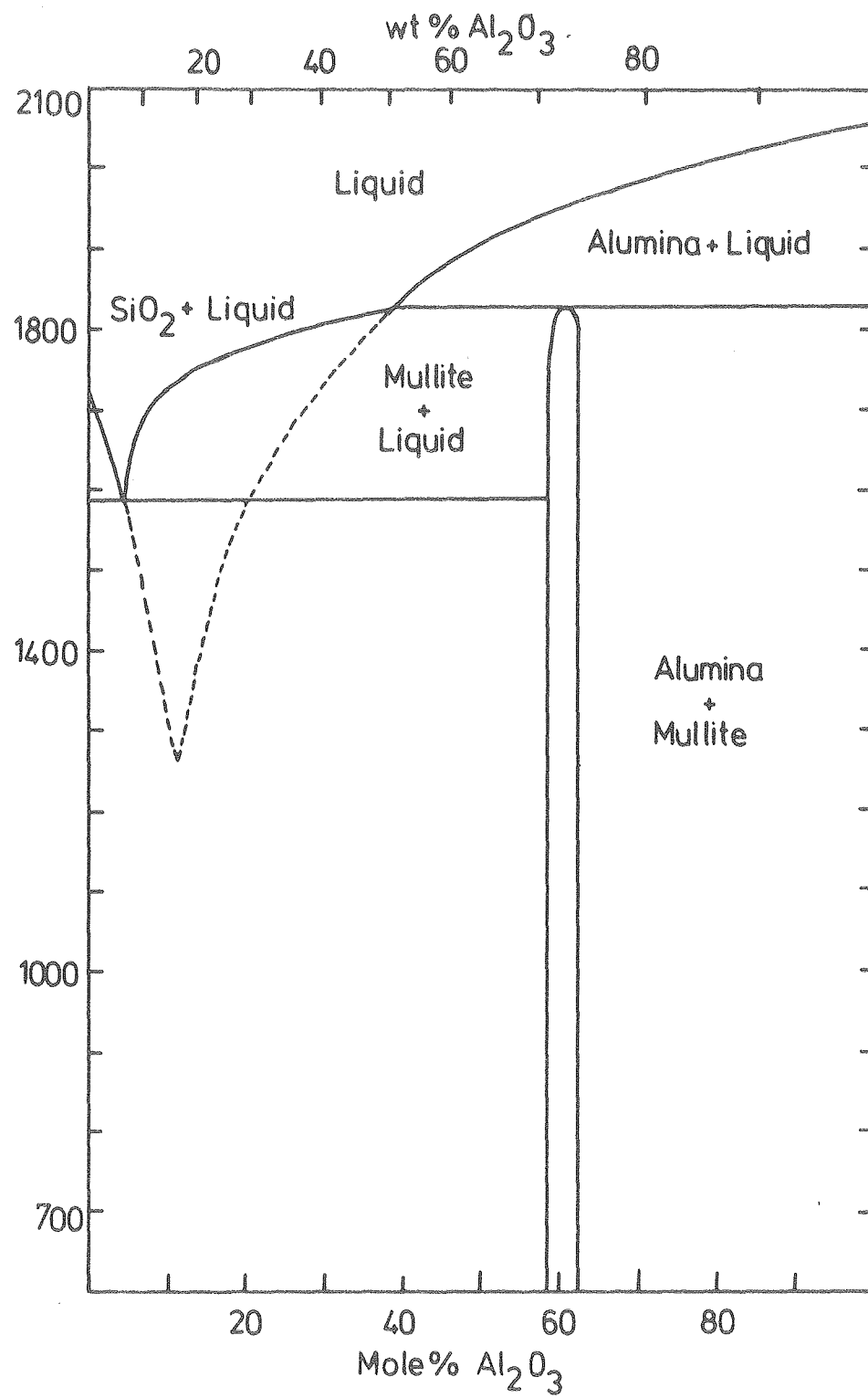
XBL 806-10227

Fig. 2-1



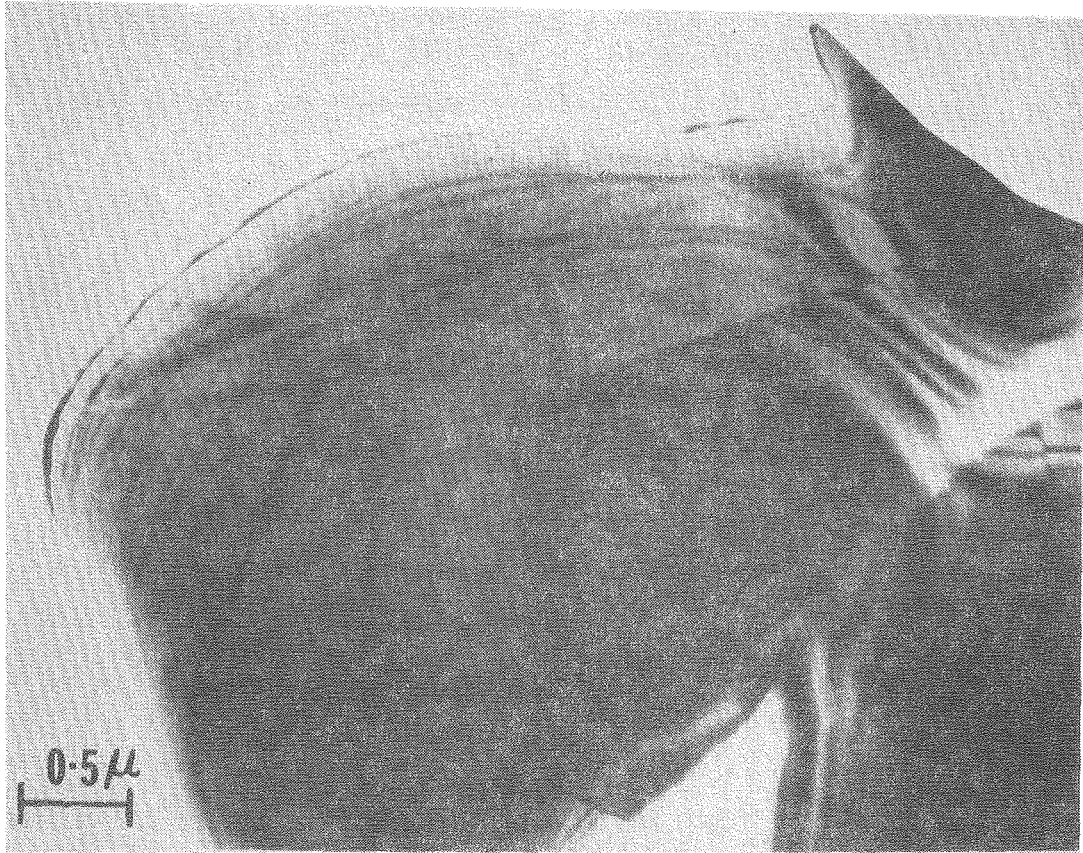
XBL 809-11787

Fig. 2-2



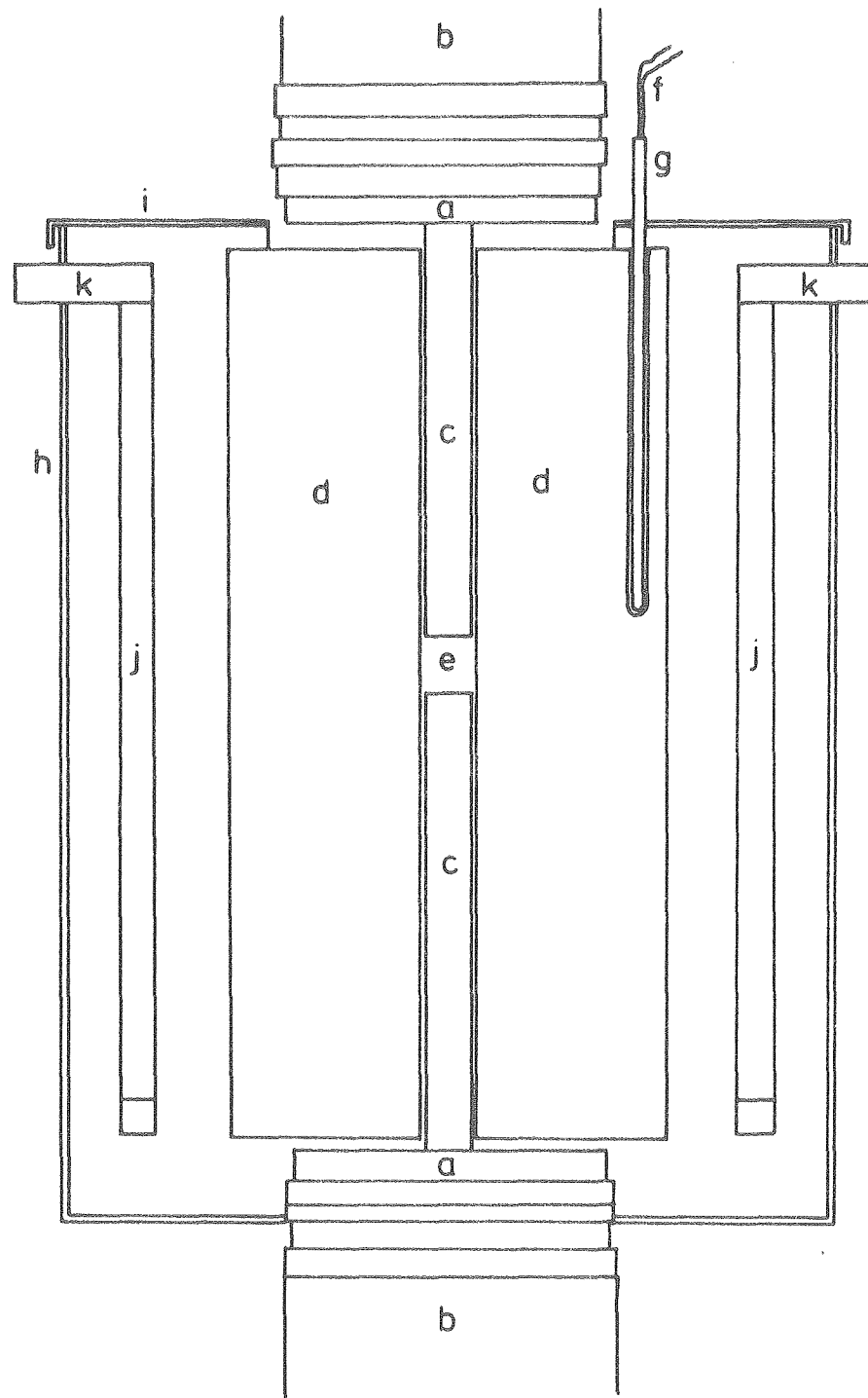
XBL 809-11685

Fig. 6-1



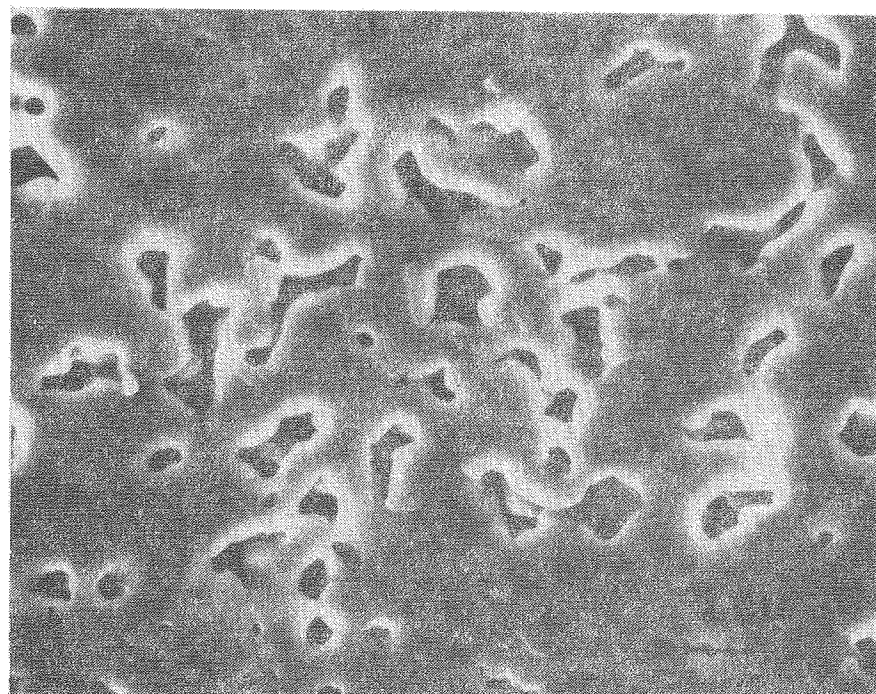
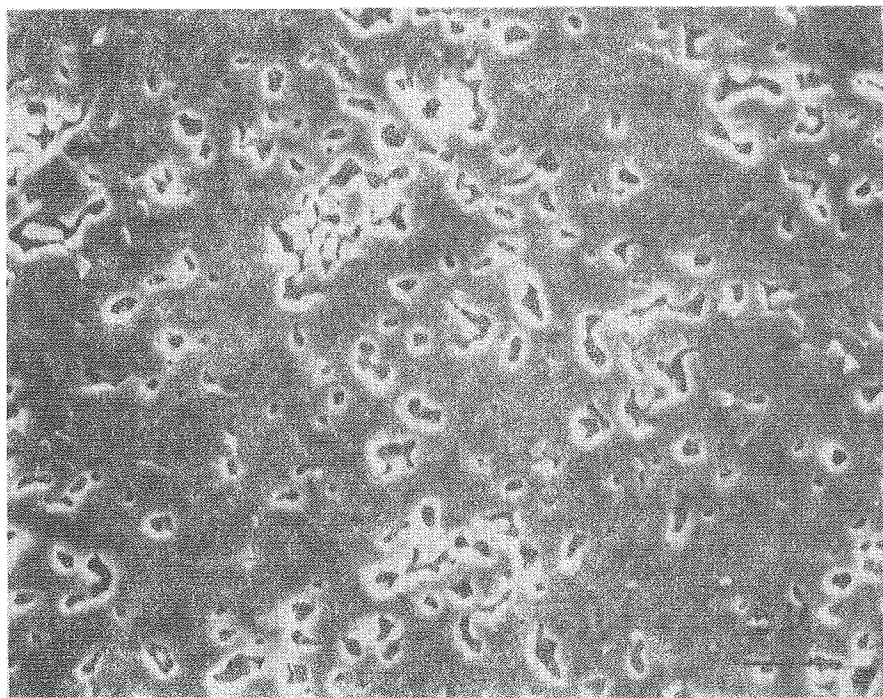
XBB 806-7166

Fig. 6-2



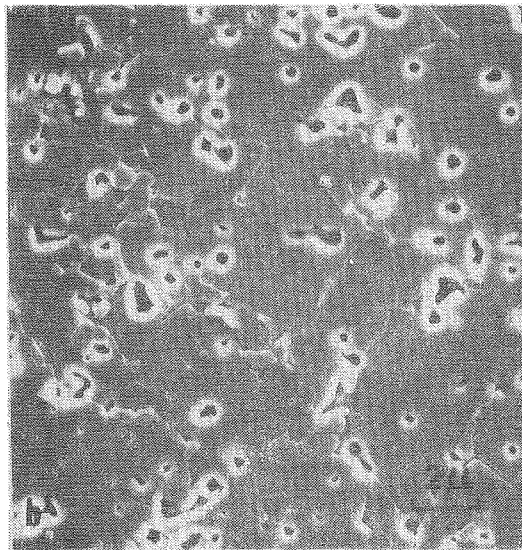
XBL 809-11689

Fig. 6-3



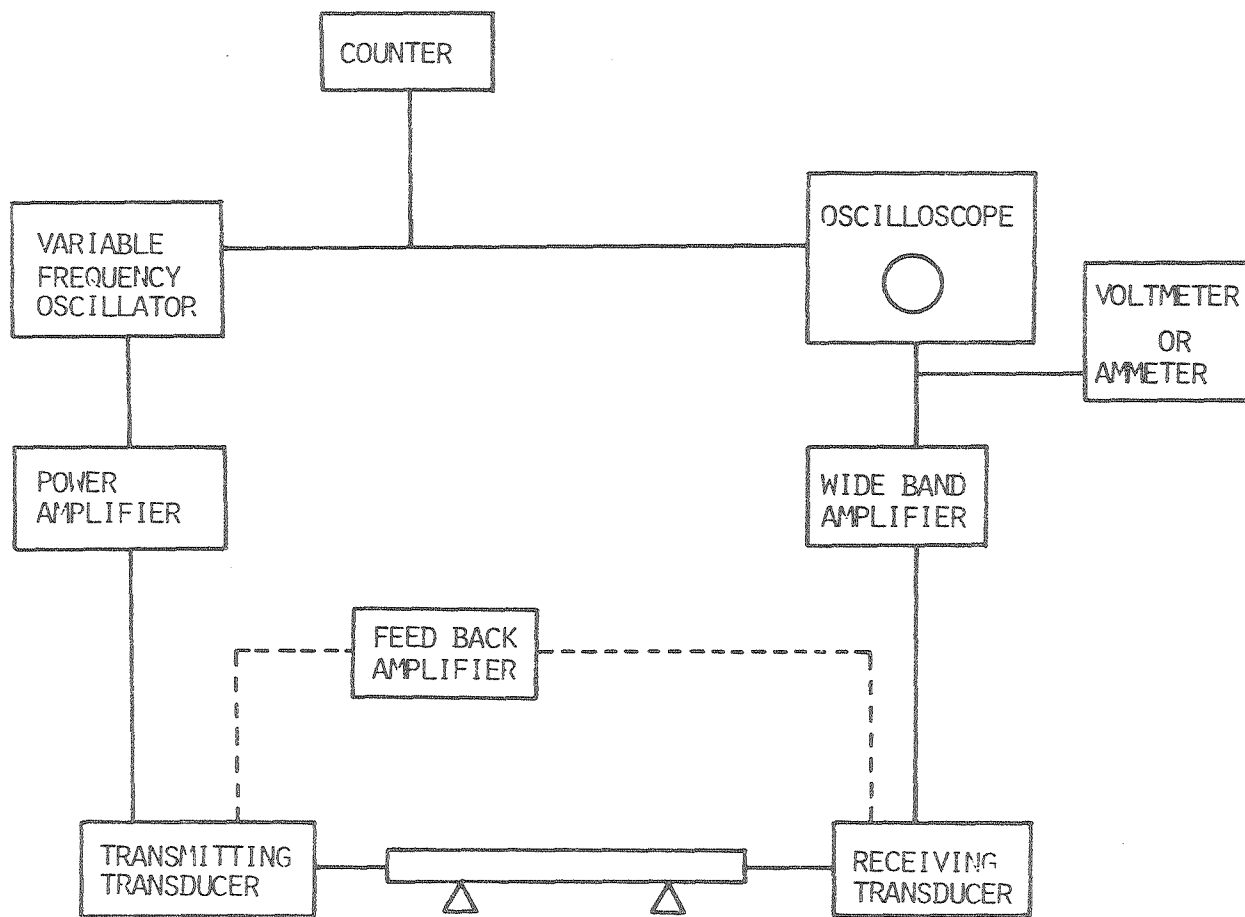
XBB 807-8233

Fig. 6-4



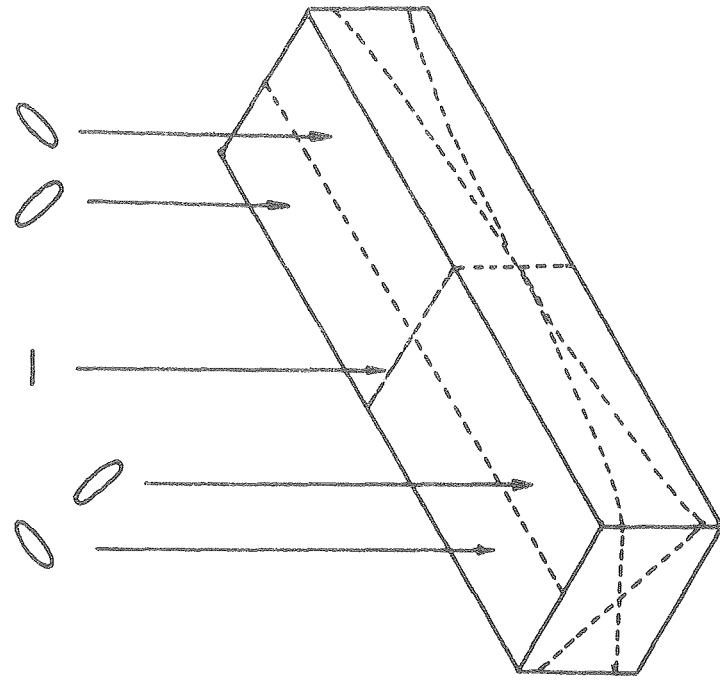
XBB 809-11041

Fig. 6-5

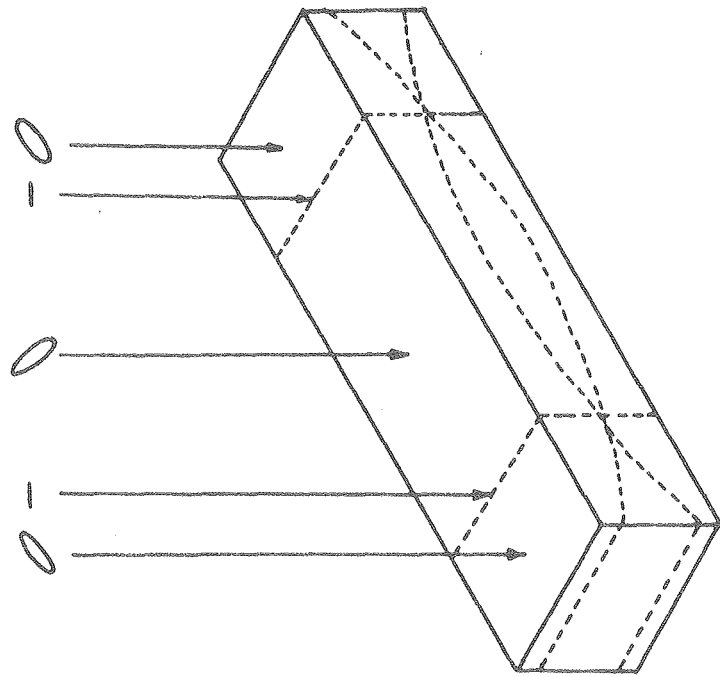


XBL 806-10228

Fig. 6-6

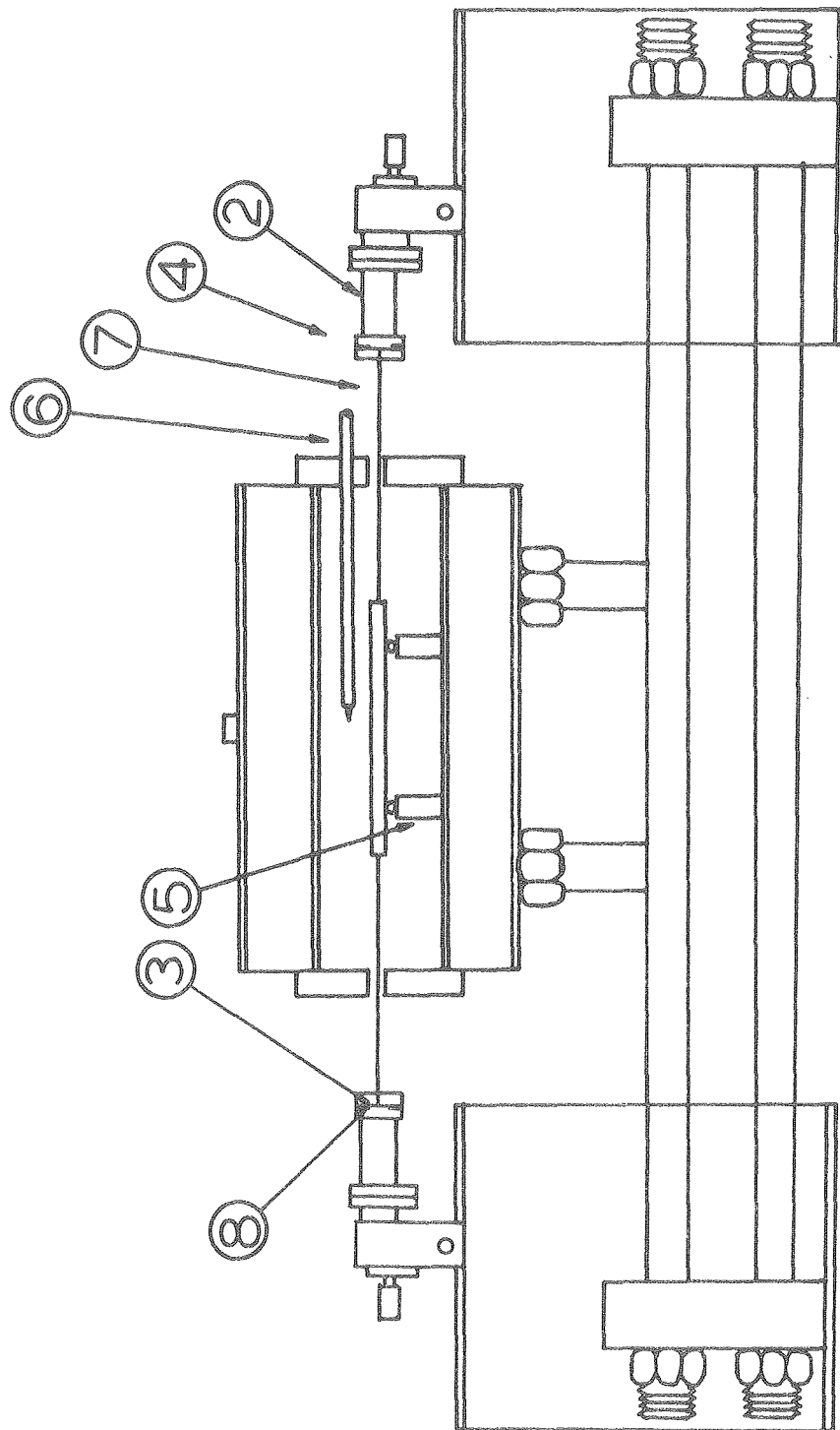


(a) Flexural vibration



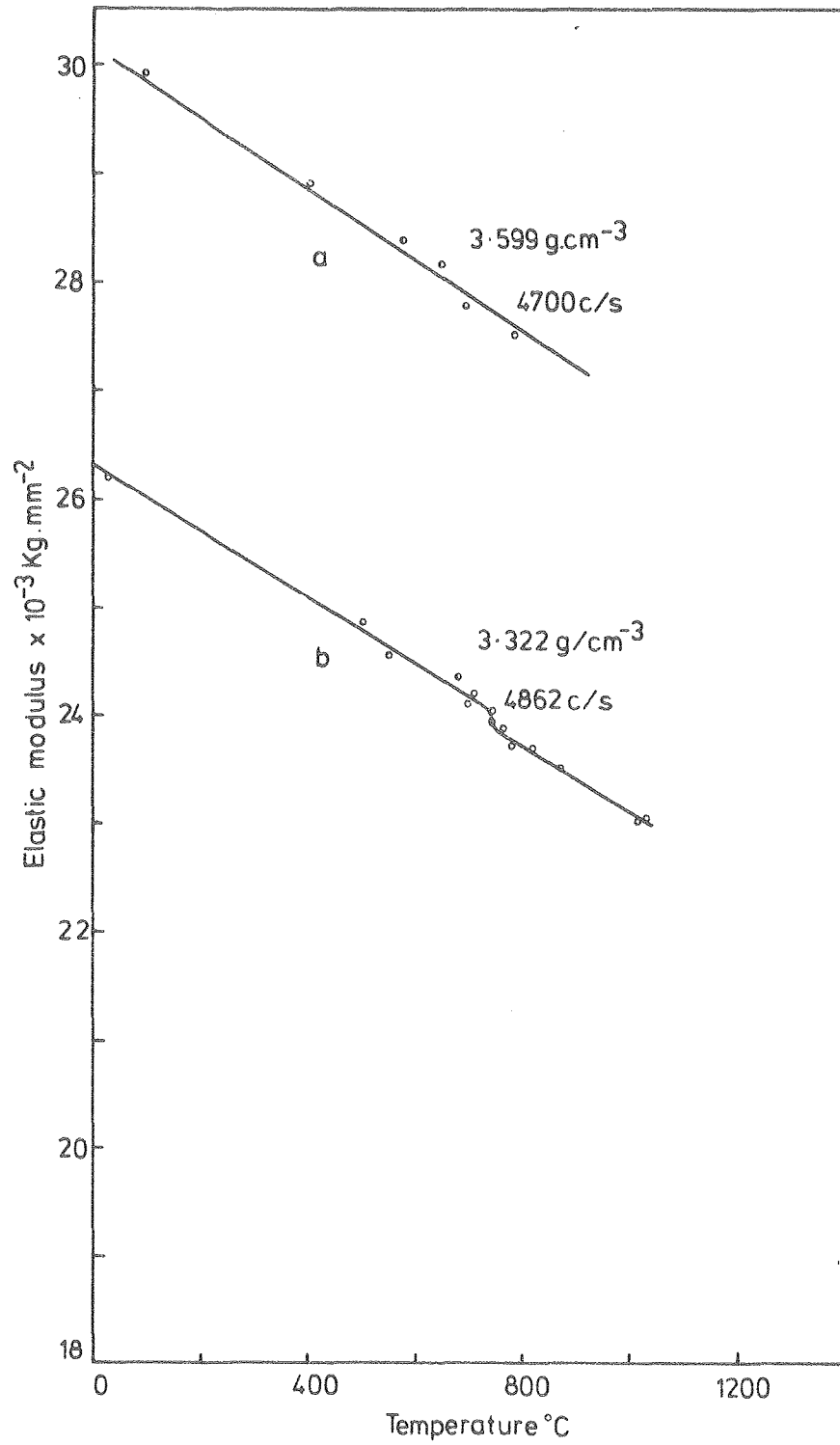
(b) Torsional vibration

XBL 809-11688



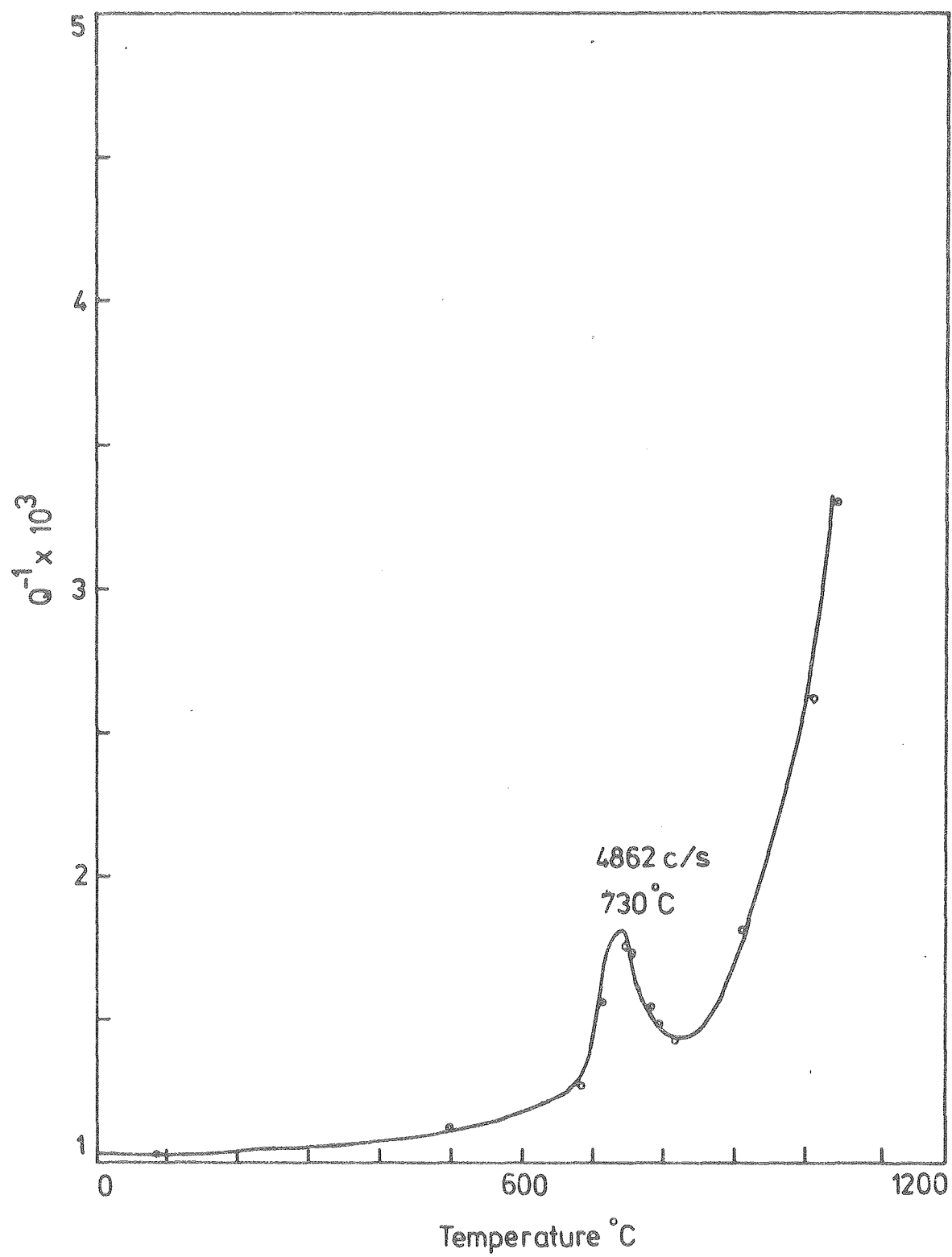
XBL 806-10229

Fig. 6-8



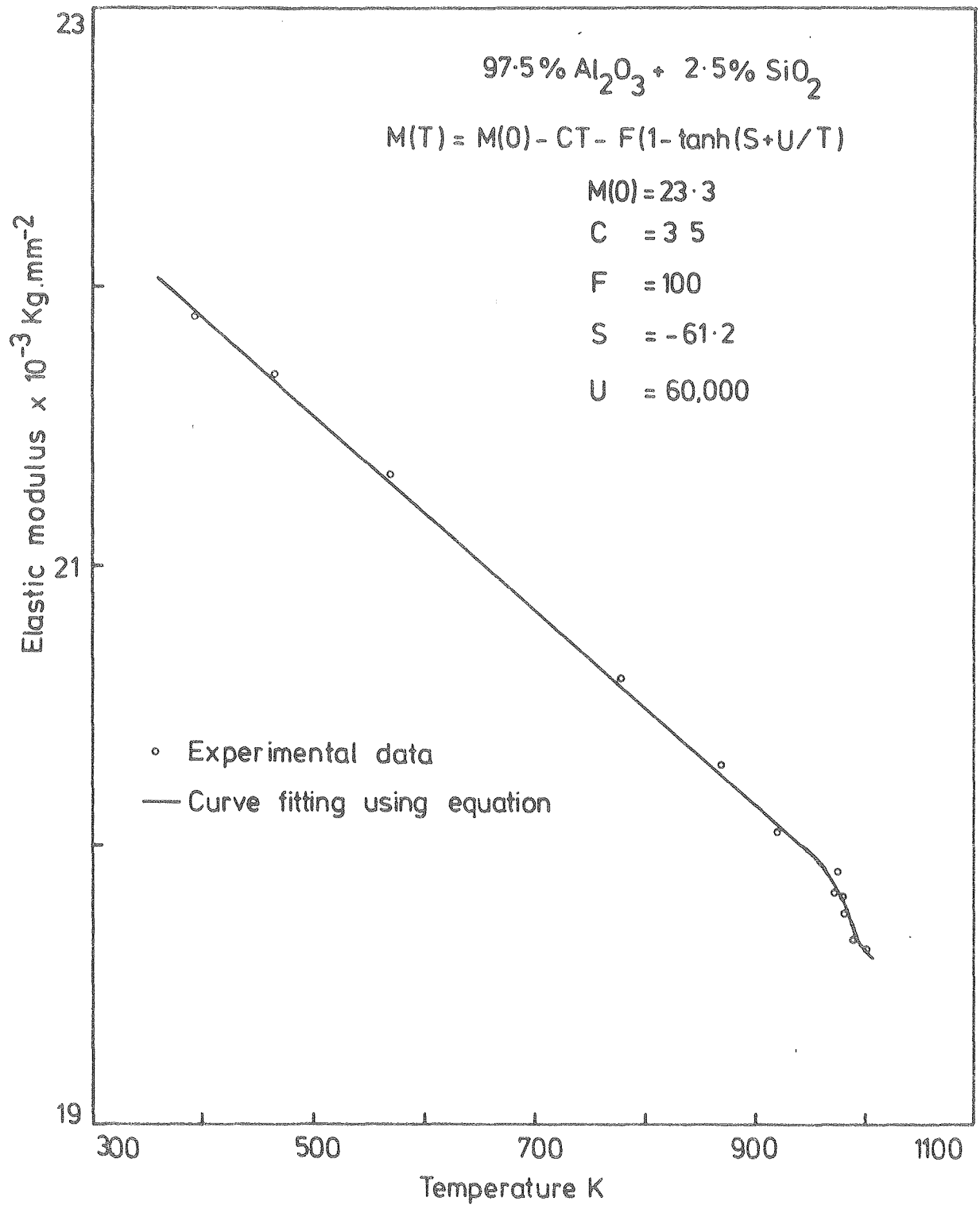
XBL 809-11682

Fig. 6-9



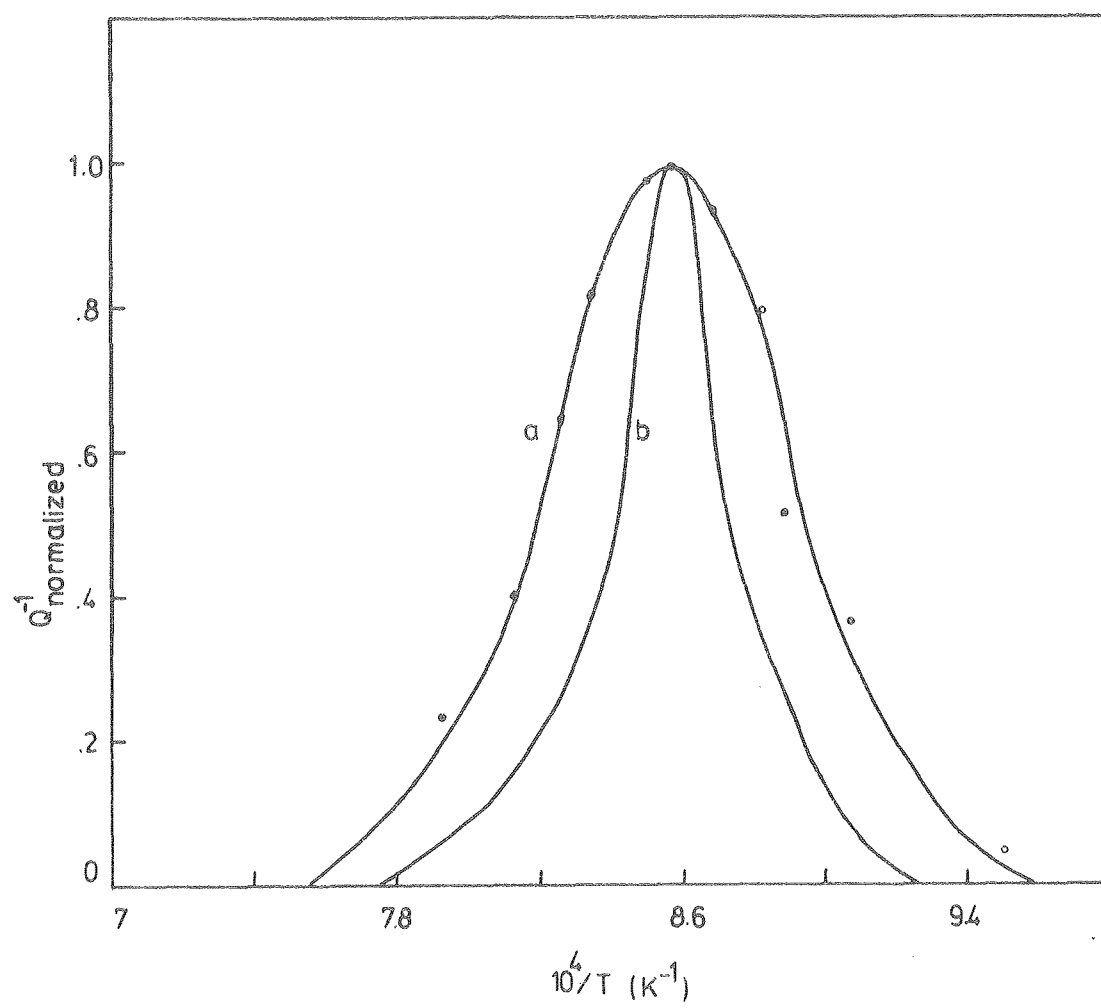
XBL 809-11687

Fig. 6-10



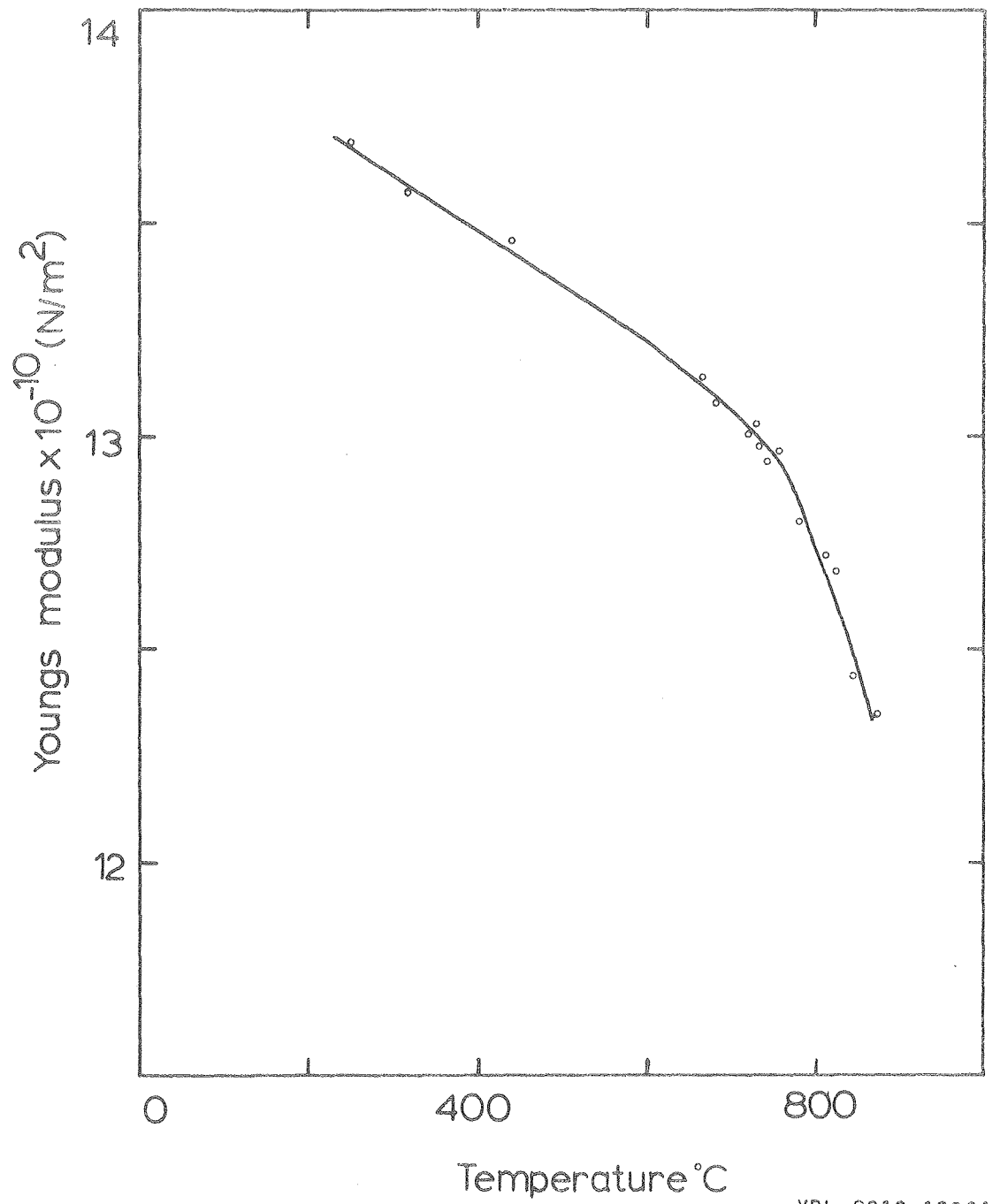
XBL 809-11691

Fig. 6-11



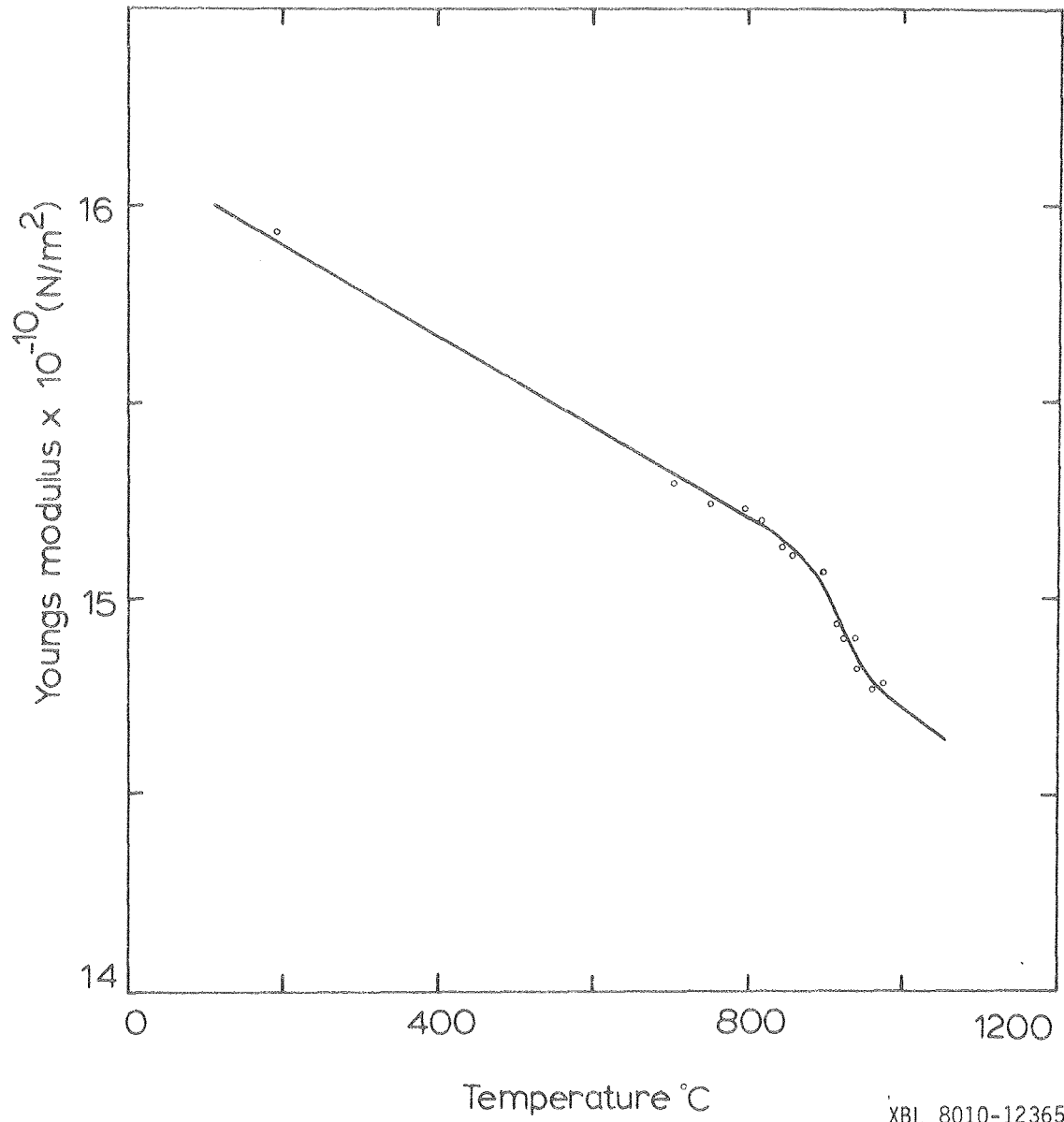
XBL 809-11690

Fig. 6-12



XBL 8010-12364

Fig. 6-13



XBL 8010-12365

Fig. 6-14

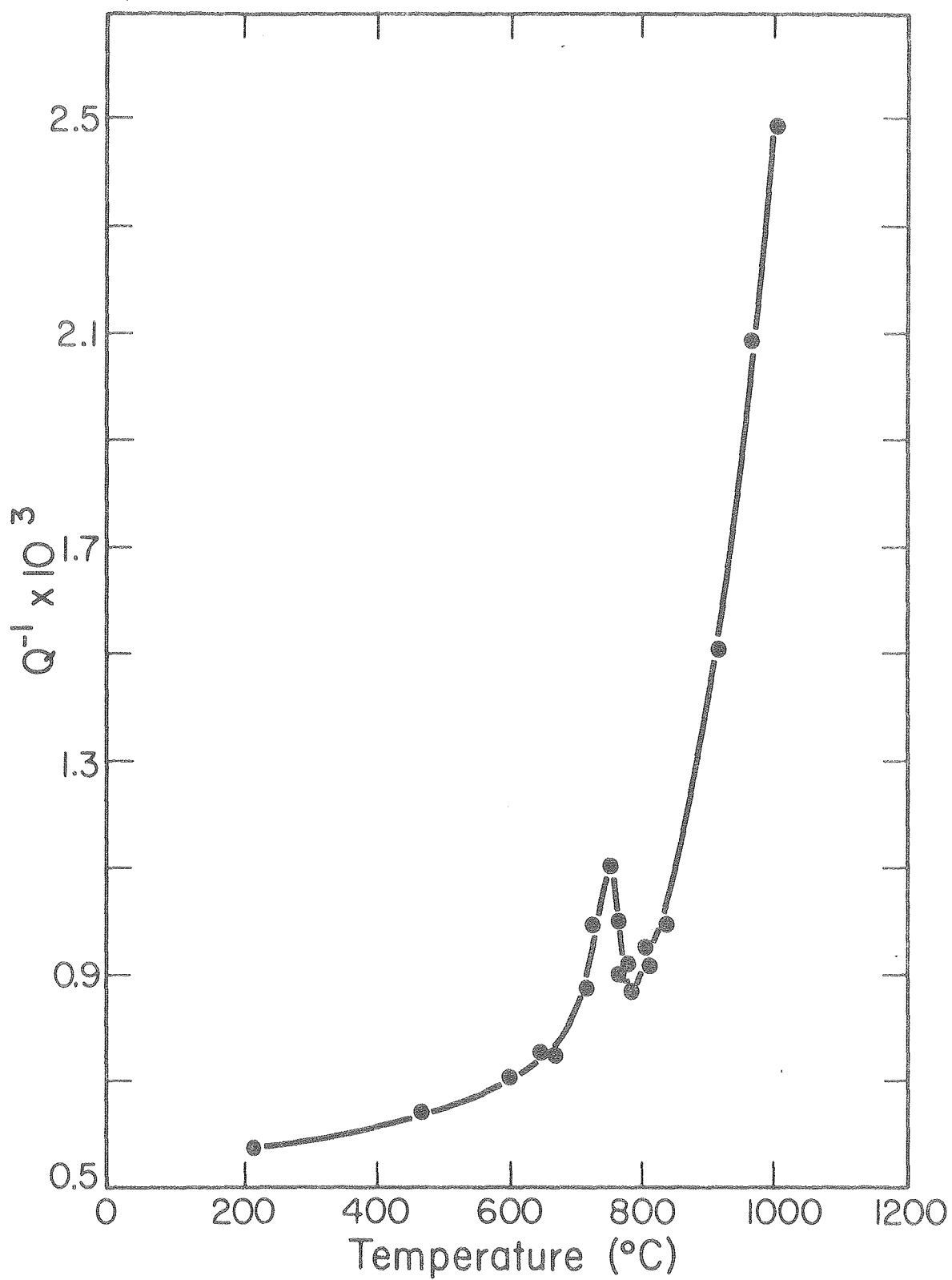
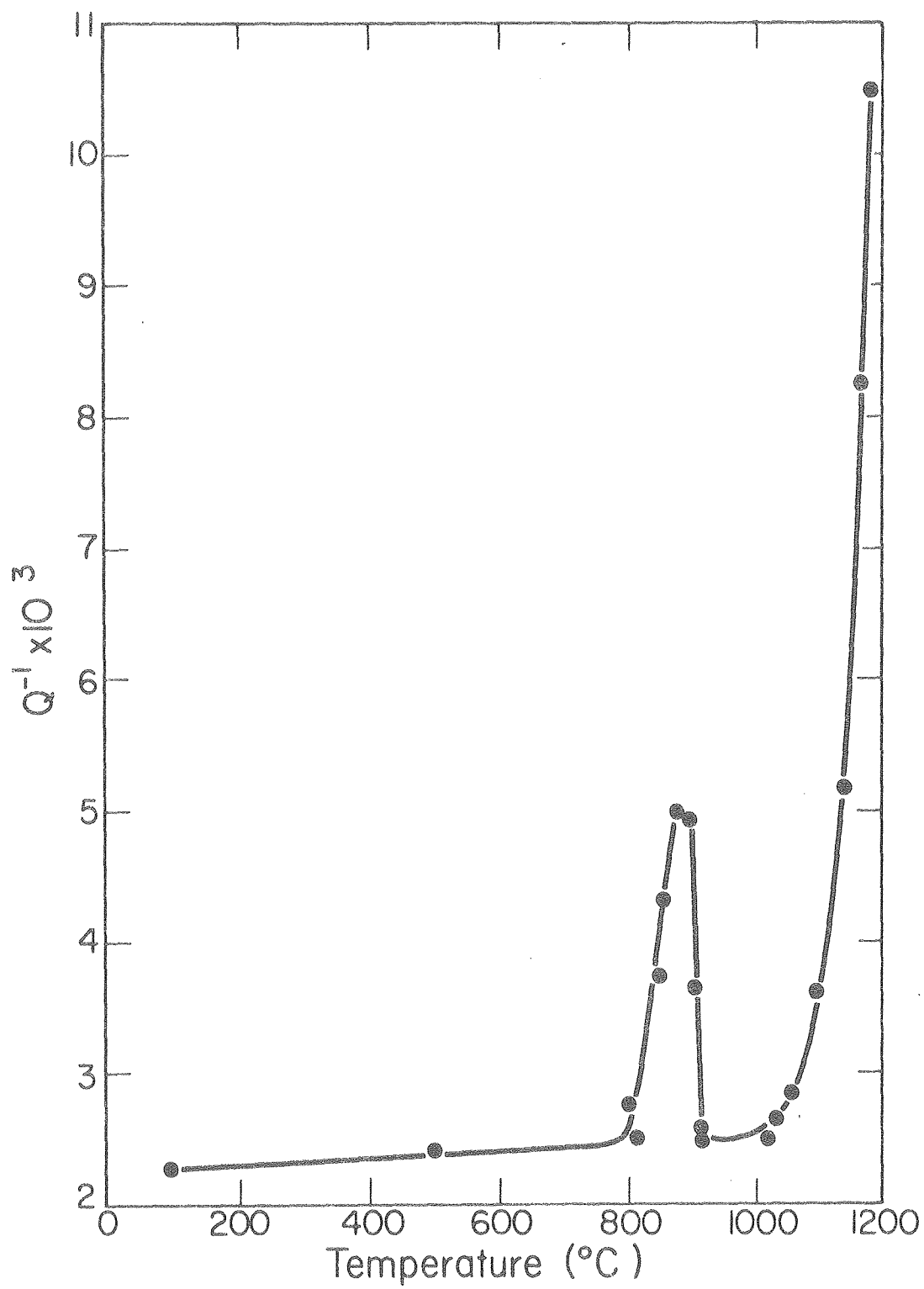


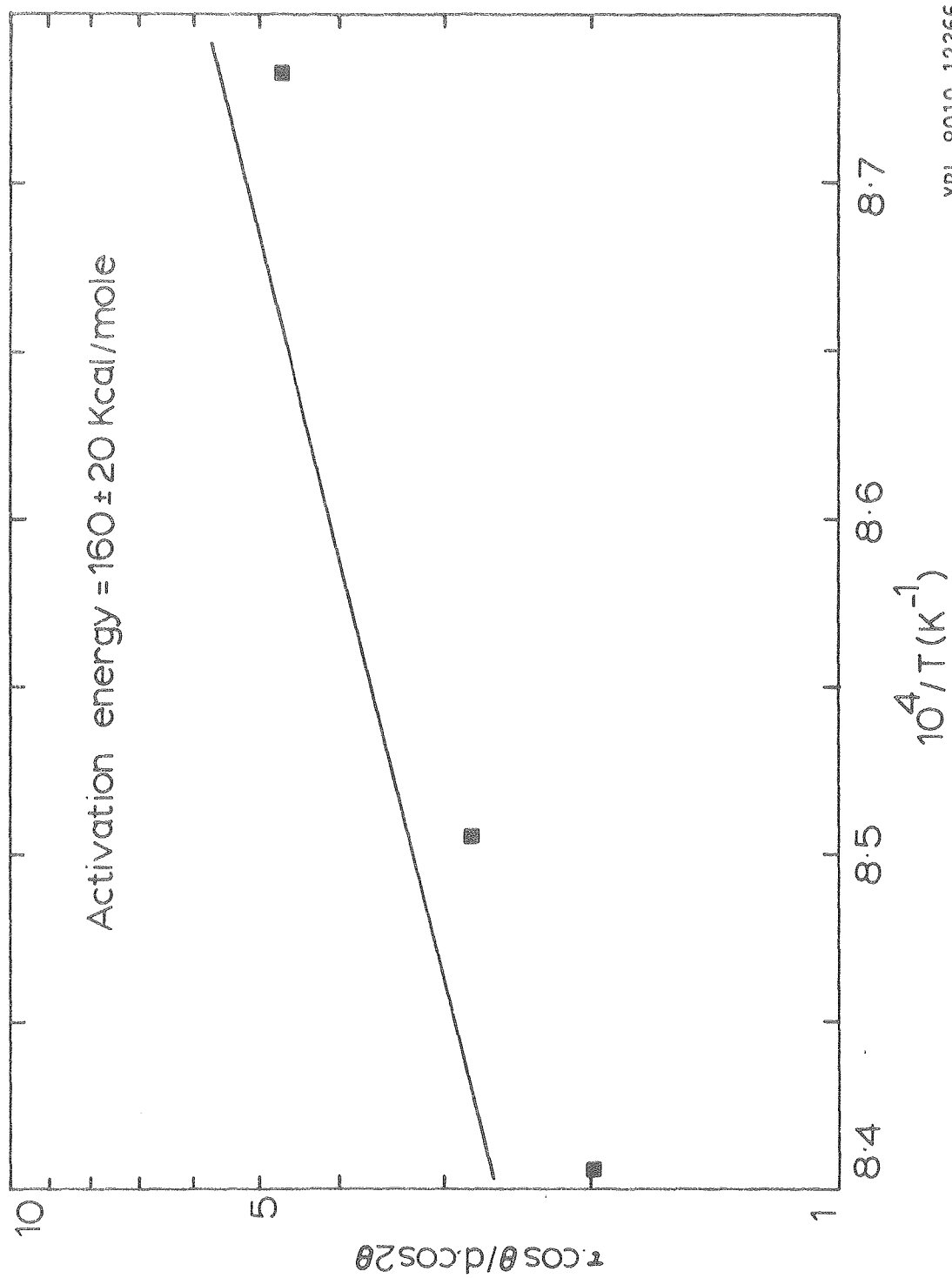
Fig. 6-15

XBL 803-421



XBL 803-422

Fig. 7-1



XBL 8010-12366

Fig. 7-2

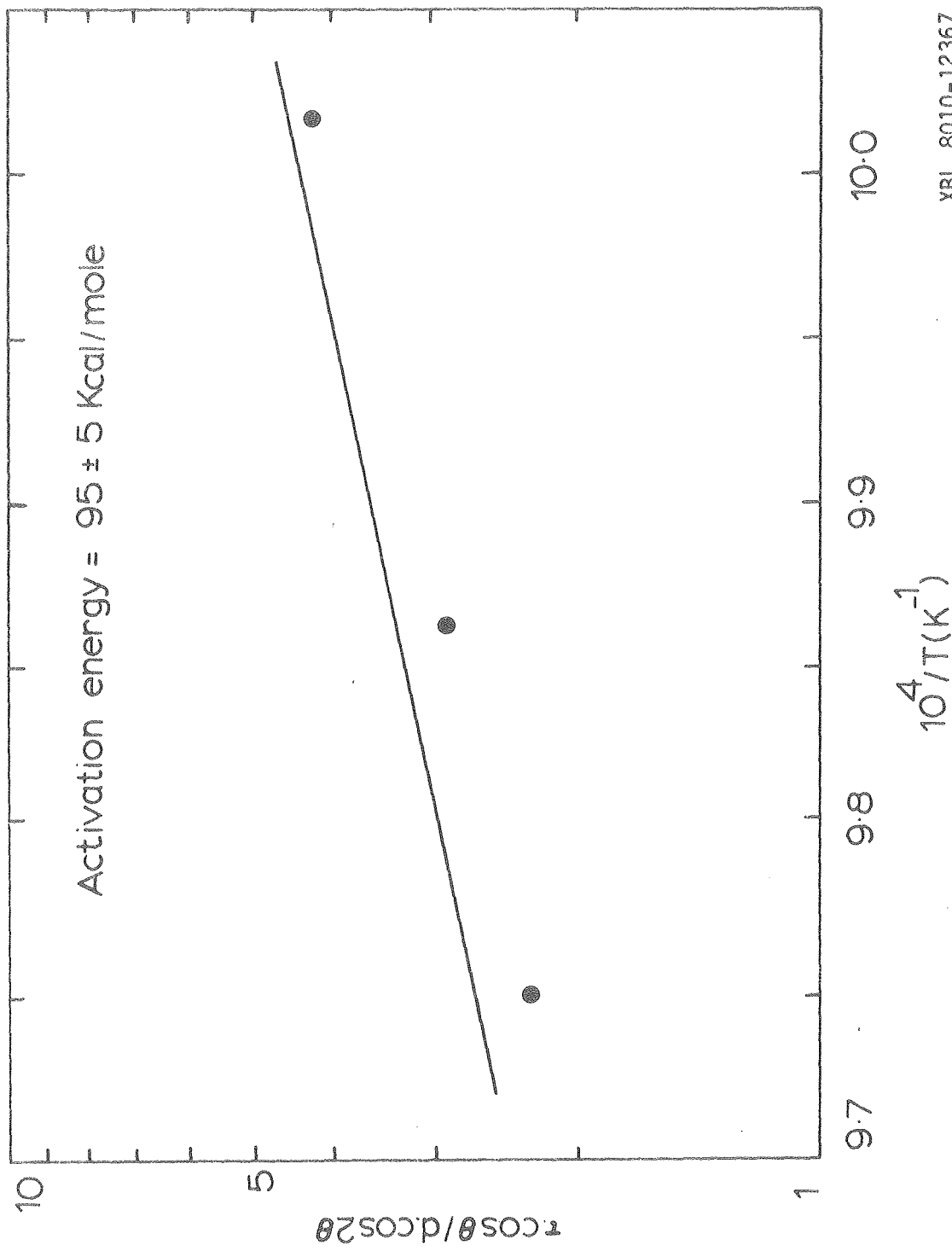
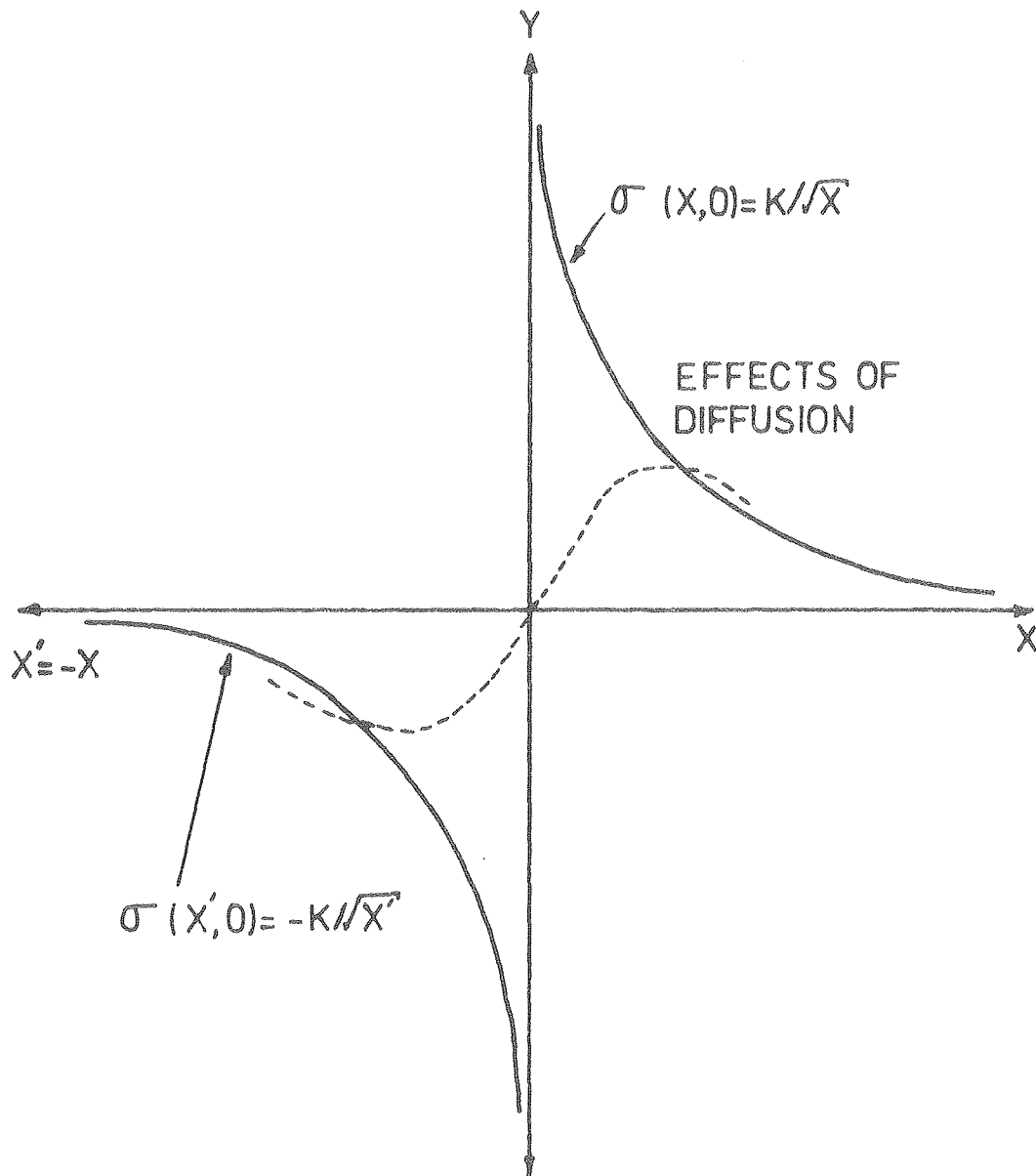


Fig. 7-3

XBL 8010-12367



XBL 809-11675

Fig. 8-2

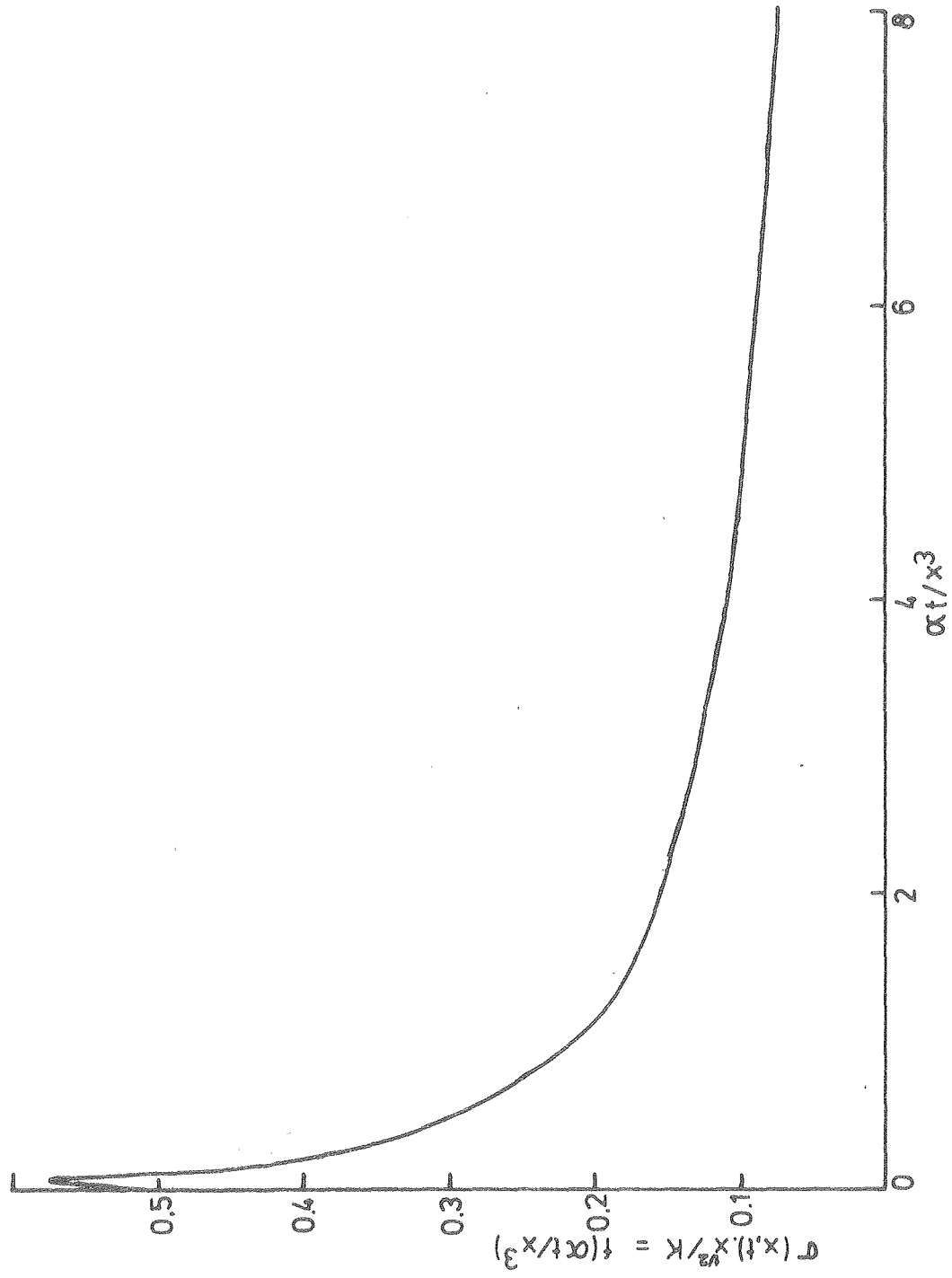


Fig. 8-3

XBL 809-11678

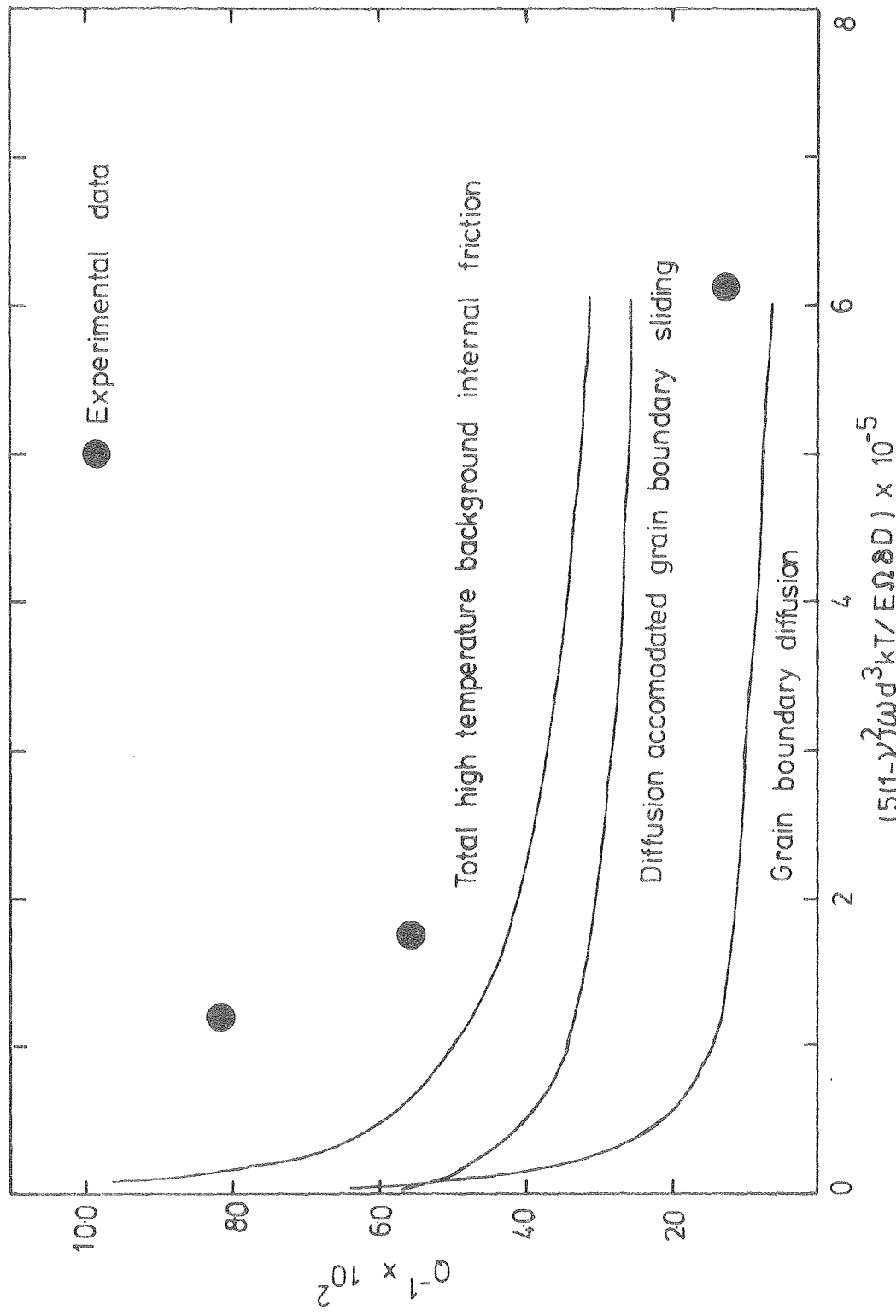


Fig. 8-4

XBL 809-11782

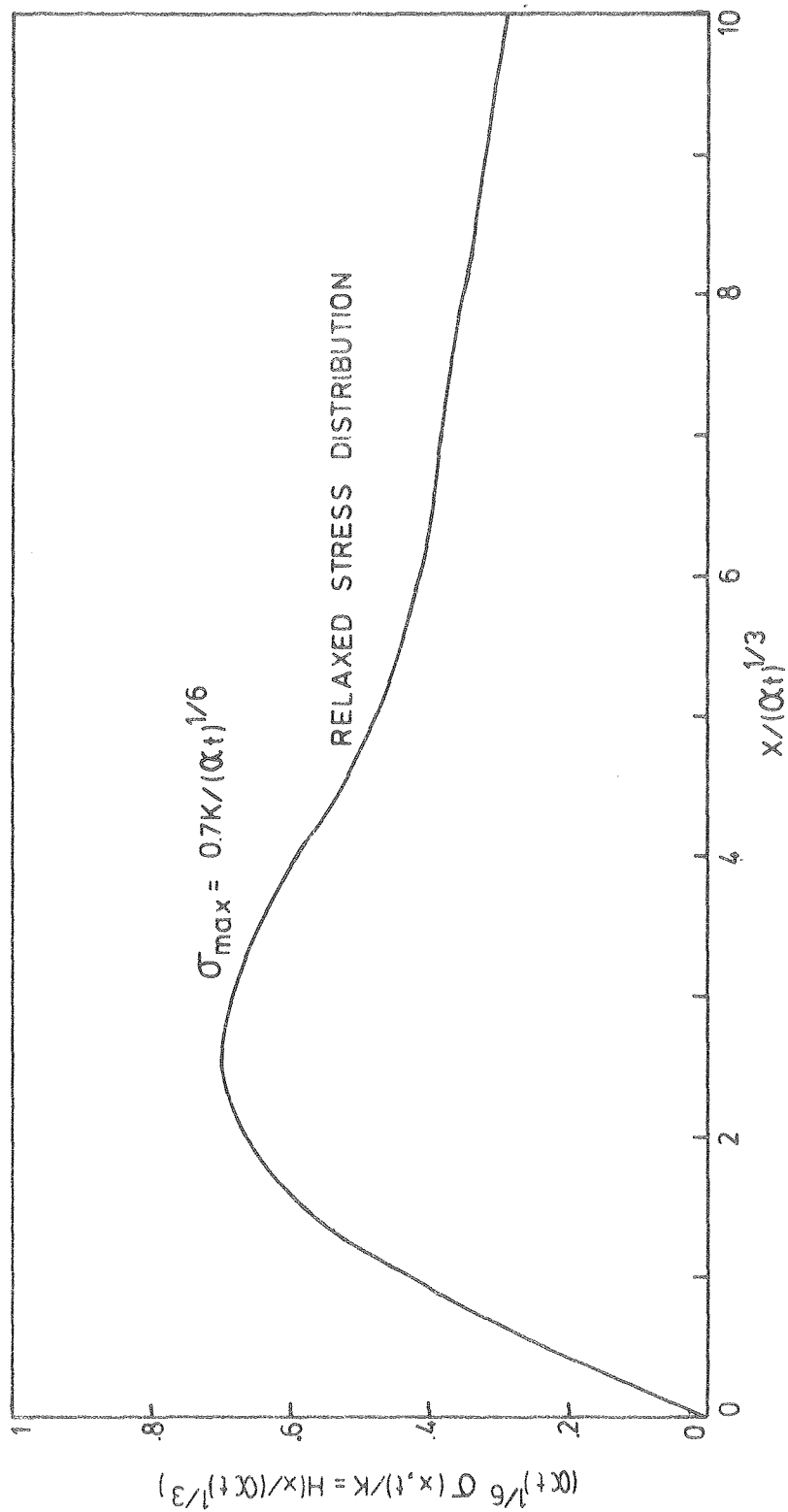


Fig. 8-5

XBL 809-11679

